7

Infrared, Light, Ultraviolet, Laser- and X-ray-Tubes

A. Ulrich, M. Born, H.W.P. Koops, H. Bluhm, and T. Jüstel

7.1 General Physics of Photon Generation

7.1.1 Historical Development

Vacuum electronic devices played a key role for our understanding of light and atoms. Besides the very early work on optical spectroscopy by Kirchhoff and Bunsen in 1860 [1] using flames, it was from the great variety of gas discharge experiments that we learned about spectral lines and their assignment to the various atoms and molecules. The practical importance of vacuum electronic devices for generating light will become obvious in the following chapters. Although the quantized nature of light is much more obvious in the discrete spectral lines emitted from low pressure gas discharge devices, the concept of the "photon" as the "quantum" of electromagnetic radiation was first introduced by Max Planck in connection with the precision of measurements of the so-called black body radiation in 1900 [2]. In this context Planck's formula (7.1) can be used for comparing other light sources with this black body radiation source at temperature T (see Fig. 7.1),

$$L_\lambda \, \mathrm{d}\lambda = \frac{2hc^2}{\lambda^5} \frac{1}{\mathrm{e}^{\frac{hc}{\lambda kT}} - 1} \mathrm{d}\lambda. \tag{7.1}$$

Here, L_λ is the power emitted per unit area, wavelength interval and solid angle. The index λ indicates that L_λ is given versus wavelength. The constants are: Planck's constant h, velocity of light in vacuum c, and the Boltzmann constant k. Studies of emission and absorption of light performed in the years following Planck's introduction of "light quanta" led to a powerful concept for the description of these processes and finally to a completely new insight into matter and its motion on a microscopic scale – quantum mechanics. It was found that both light and matter contains aspects of waves and particles. The link between these two aspects is described by a relation between wavelength λ or wave vector $\boldsymbol{k}$ ($\boldsymbol{k} = 2\pi/\lambda$) and frequency ν on one side and momentum p and energy E on the other side,

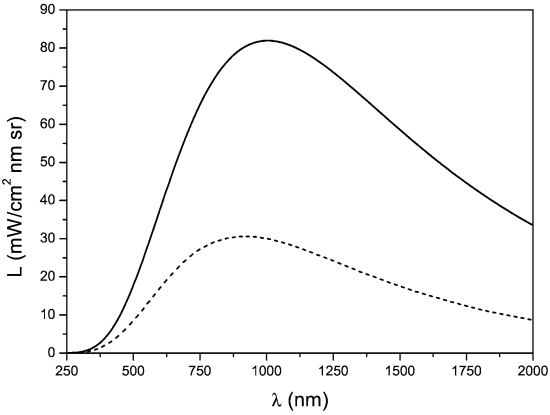

Fig. 7.1. Emission from a black body at a temperature of 2600 K (*solid line*). The emission from a tungsten strip calibration lamp (OSRAM, type Wi17g, No. 2892) with the same radiative temperature is shown for comparison. The difference is due to the finite emissivity of tungsten as measured by J.C. de Vos [3]

$$E = h\nu, \quad \vec{p} = \hbar \boldsymbol{k}. \tag{7.2}$$

The reader is asked to refer to publications about quantum mechanics for a deeper discussion of these fundamental aspects of light and matter. The important result obtained from quantum mechanics, in this context, is that bound systems, such as electrons orbiting around a nucleus, have well defined, discrete energy levels. Emission and absorption of light quanta (photons) of energy $E = h\nu$ is a possibility for the systems to make transitions from one energy level to another when the energy difference between the levels is the same as the photon energy E.

To a level of accuracy which is normally sufficient to represent all practical aspects of light sources, including lasers, the energy levels of atoms and molecules can be described by non-relativistic quantum mechanics. Coupling of these potentially light emitting or absorbing species with an electromagnetic radiation field can be described by the so-called Einstein coefficients A and B. Techniques for calculating the quantum mechanical eigenstates and energy eigenvalues of light emitting species are not discussed here. Energy levels of atoms are usually organized by main quantum numbers, quantum numbers of spin, and angular momentum. Total angular momentum is described by a quantum number J. For most practical applications energy levels of atoms can be found in tables [4, 5]. Phenomenologically, molecular levels are organized by electronic excitation (normally named X for the ground state and A, B, C, etc. for excited states), a vibrational quantum number v and a rotational quantum number I. The combination of electronic-, vibrational- and rotational energy can be calculated from parametrized descriptions of the molecular potential curves. The parameters for diatomic molecules can be found in tables [6].

Light emission from a light source is initialized by promoting atoms or molecules in the device from the ground state into an excited state, normally via collisions with

electrons. It should be noted that several eigenstates of an atom or molecule may have the same energy. An "energy level" may therefore consist of several "states". Such an energy level is said to be degenerated with a degeneracy g if g states have this particular energy. An excited species will have the tendency to return to the ground state releasing the excitation energy to its surroundings either by collisions with other species or by emitting a photon. It is the "art" in designing a light source to make photon emission in the desired wavelength region a dominant and efficient process in the device.

The process by which an undisturbed atom or molecule undergoes a transition from a level i to a level k via photon emission is called *spontaneous emission* and is governed by the Einstein coefficient A_{ik}. It has the unit 1/s and is a measure for the probability $\mathrm{d}P_{ik}$ of an atom to make the transition within a certain time interval $\mathrm{d}\tau$ ($\mathrm{d}P_{ik} = A_{ik}\,\mathrm{d}\tau$). It can therefore be used to calculate the time dependence of the number N_i of species in the upper level i starting from an initial number N_{i0},

$$N_i = N_{i0}\mathrm{e}^{-A_{ik}\tau}, \tag{7.3}$$

if photon emission is the only decay mode and the species decay independently of each other. The Einstein coefficient A_{ik} values can be calculated from basic principles in quantum mechanics. For practical applications one can refer to tabulated A_{ik} values [7]. The energy E (frequency ν, wavelength λ) of the photon emitted in this process is related to the energy difference between level i and k,

$$E = h\nu = hc/\lambda = E_i - E_k. \tag{7.4}$$

The energy level with higher energy E_i is often referred to as "upper" level and the level with lower energy E_k as "lower" level.

Resonant *absorption* is a process in which a photon is absorbed by an atom or molecule inducing a transition from a lower energy level k to a level i of higher energy. The photon energy E has to meet the requirement $E = E_i - E_k$. The probability for a given species in state k to be promoted to state i via absorption of a photon is proportional to the Einstein coefficient B_{ki} and the energy density $u(\nu)$ of the electromagnetic radiation field providing the photons which can be resonantly absorbed.

A third fundamental process is resonant interaction of a photon with an atom or molecule in the upper level i forcing it to the lower level k. It is called *stimulated emission*, and the radiation which is created is coherently superimposed on the radiation stimulating the transition. This means that the electromagnetic energy released in the transition travels in the same direction and is in phase with the incident radiation. Because of its similarity with the absorption process where radiation stimulates an "upward" (k to i) transition the process is described by a coefficient B_{ik} for the "downward" (i to k) transition. The transition probability is proportional to the coefficient B_{ik} and the energy density $u(\nu)$ of the radiation field.

In summary, the three processes for emission and absorption of photons are visualized in Fig. 7.2. To calculate the number of emission and absorption processes per unit volume and time interval for a specific transition, the density of species in the

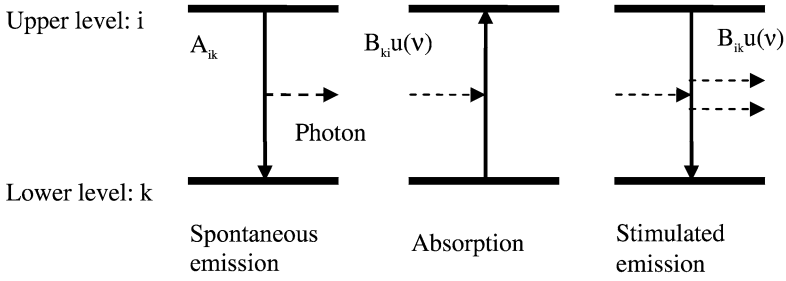

Fig. 7.2. Principle processes of light emission and absorption

upper and lower level N_i and N_k have to be known. These densities can be obtained from rate equations describing the rates at which species with energy E_i and E_k are populated and depopulated. The rates by which two selected level densities N_i and N_k change via photon emission and absorption can be obtained from the Einstein coefficients A_{ik}, B_{ik}, and B_{ki} which have been introduced above:

$$\mathrm{d}N_i/\mathrm{d}t = -A_{ik}N_i - B_{ik}N_i u(\nu) + B_{ki}N_k u(\nu)$$

and

$$\mathrm{d}N_k/\mathrm{d}t = A_{ik}N_i + B_{ik}N_i u(\nu) - B_{ki}N_k u(\nu). \tag{7.5}$$

The Einstein coefficients are related to each other in the following way:

$$g_i B_{ik} = g_k B_{ki} \text{ and } A_{ik} = (8\pi h\nu^3/c^3)B_{ik}. \tag{7.6}$$

So far a perfect resonance between the radiation field and the absorbing or emitting species has been assumed. In many cases, however, the detailed frequency dependence of the absorption-, emission-, and optical-gain in the narrow frequency region of a spectral line has to be taken into account. Various broadening effects such as Doppler- and pressure broadening influence the line shape. This can be described by a line shape function $g(\nu)$ which is normalized as

$$\int g(\nu)\,\mathrm{d}\nu = 1. \tag{7.7}$$

A beam of radiation with a specific frequency ν and intensity I (in units W/m^2) which interacts over a distance x with the atoms and molecules varies its intensity according to

$$I = I_0 \exp(-k(\nu)x). \tag{7.8}$$

The absorption coefficient $k(\nu)$ depends on the values defined above as

$$k(\nu) = \sigma(\nu)((g_i/g_k)N_k - N_i). \tag{7.9}$$

The absorption cross-section is given by

$$\sigma(\nu) = \frac{\lambda^2 A_{ik}}{8\pi\eta^2} g(\nu), \tag{7.10}$$

where η is the index of refraction of the medium. Note that relation (7.9) describes both absorption and stimulated emission. When the term $((g_i/g_k)N_k - N_i)$ becomes negative because $N_i > g_i/g_k N_k$, the intensity I will grow exponentially in the excited medium. This "**L**ight **A**mplification by **S**timulated **E**mission of **R**adiation" is the basic process of the device known as "LASER".

This brief introduction to the light emission and absorption processes allows important parameters, such as the power emitted from a lamp or the small signal gain of a gas laser tube, to be calculated.

The output characteristics of a discharge lamp could for example be estimated as follows. The emitted spectrum is given by the energy levels and corresponding transitions of the light emitting species. If absorption can be neglected, the power emitted per unit volume on a specific transition from level i to level k is

$$P/V = N_i h\nu A_{ik} \text{ with } h\nu = E_i - E_k. \tag{7.11}$$

If E_i, E_k, and A_{ik} are known from tables, the only remaining parameter which has to be determined is the density of species in the upper level i. This, however, may not always be an easy task. If N_i is not measured experimentally, a whole set of rate equations for all relevant collisional and radiative processes filling and depleting levels i and k have to be solved for obtaining a rather accurate prediction of N_i. Note that collisional processes between electrons and atoms, ions and atoms, etc. are studied as a field of its own [8]. Gain on an optical transition between two levels i and k in a gas laser tube can be predicted by a similar approach determining the population densities N_i and N_k and calculating the gain using (7.9) and (7.10).

7.2 Laser

7.2.1 Introduction

"Light Amplification by Stimulated Emission of Radiation" (LASER) was first observed by Maiman in 1960 using a flash lamp pumped ruby crystal as the laser medium [9]. Also, in that year Javan et. al. built the first gas laser with a discharge pumped low pressure He–Ne mixture as the laser medium and observed laser effect in the near infrared region [10]. Since that time one branch of laser development is based on vacuum electronic devices. The interesting history of the invention of lasers and masers was described by Charles Townes [11]. The variety of lasers which have been developed since its invention is overwhelming. Here, a short review of gas lasers which are of practical importance is given.

The general operation principle of light amplification in matter has been described in Sect. 7.1.1. The main prerequisite for getting a laser to operate is to achieve "population inversion" $(g_k/g_i)N_i > N_k$ (formula (7.9) in Sect. 7.1.1). The term inversion refers to the fact that at normal, thermal equilibrium conditions the population density N_k of the lower level is always higher than the population density N_i of

the energetically higher lying level. The "art" of laser design is to create conditions which are far away from thermal equilibrium in the sense that the N_i/N_k ratio is different from its value at thermal equilibrium, at least for two specific levels i and k. Optical feedback in the form of an optical resonator is another main ingredient for getting a gas laser operational, although some lasers like the 337 and 358 nm ultraviolet nitrogen lasers and so called soft X-ray lasers make use of light amplification in one pass through the device. Fabry–Perot type optical resonators consisting of two mirrors are normally used. Both flat and curved mirrors can form an optical cavity.

Balance between optical gain and losses in the resonator determines whether or not intensity will build up in a particular mode. Losses are due to absorption in all optical elements in the resonator, finite reflection of the laser mirrors and diffraction on the apertures of the device. Laser threshold is reached when the gain α is equal to the loss γ for light making one round trip in the resonator,

$$\alpha = \gamma.$$

Maximum small signal gain α_0 in the line center ν_0 is given by

$$\alpha_0 = \sigma(\nu_0)(N_i - (g_i/g_k)N_k).$$

The cross-section for stimulated emission $\sigma(\nu)$ is defined in (7.9) and (7.10) of Sect. 7.1.1.

Extraction of light from the laser resonator contributes to the losses of the resonator. Semitransparent laser mirrors are frequently used for extracting a certain fraction of the light intensity which builds up in the resonator during laser operation. If the amplification of light in the laser medium can be maintained over a period of time which is longer than the decay time of light in the resonator, the characteristics of the decoupled light beam are governed by the parameters of the optical resonator. A discussion of line shapes and line broadening effects can be found in the literature on lasers and atomic physics [12]. Detailed descriptions of optical gain in a laser medium and the modes of an optical resonator are, for example, given in [12] and [13].

Finding new laser media and laser transitions followed the invention of the laser. Over 6100 lines are listed [14, 15]. Compilations of original papers on gas laser technology and short wavelength lasers have been published [16, 17]. Only a few lasers are commercially successful.

7.2.2 Specific Laser Devices

A general advantage of gas lasers is that the optical properties of the laser medium are not permanently damaged by its operation. An overview over widely used gas lasers is given in Table 7.1. This allows high power levels in both pulsed and continuous wave (cw) lasers. However, a potential build up of impurities and overheating of the laser gas has to be avoided. The CO_2 laser in the infrared region at wavelengths around 10 μm is very efficient and often used in industrial processes for cutting and welding.

The *He–Ne laser* uses an energy resonance between helium atoms in the metastable state and neon atomic levels for achieving population inversion. Collisions of excited helium atoms with ground state neon atoms lead to selective excitation of these neon levels. The slight energy differences between the levels are compensated by the kinetic energy of thermal motion [12]. Note that the older Paschen notation is used in many early publications for the NeI levels. Racah notation is used here.

Helium–neon lasers use the positive column of a glow discharge as the laser medium. The tubes are made from glass with typical inner diameters of 1 to 2 mm. Large area cold cathodes are used. The cathode is often placed in an outer tube with

Table 7.1. Laser systems and their characteristics

Laser	Level transitions	Wavelength	Pumped by	Speciality/ output
He–Ne metastable states 7:1 He–Ne mixtures	$5s'[1/2]^0_1$–$3p[1/2]_1$ $5s'[1/2]^0_1$–$3p'[3/2]_2$ $4s'[1/2]^0_1$–$3p'[3/2]_2$	543.516 nm 632.816 nm 1.1529 µm	gas discharge dc-currents 10 mA to 50 mA; gas pressure 1 mbar	tube diameter 1–3 mm; output mW
Krypton ion	triply ionized	176 nm	low pressure discharge	
Argon ion	$3s^2p^5\ ^2P^0_{1/2}$ and $^2P^0_{3/2}$ 4p ($^2S^0$, $^2P^0$, $^2D^0$, $^4D^0$)–4s ($^2P_{1/2}$, $^2P_{3/2}$)	Vis to near UV 440 nm to 500 nm	two step process of forming and exciting the ions via electron collisions; discharge currents 30 A; pumps others	tens of Watts; output increases quadratically with discharge current
Excimer lasers Ar, Kr, Xe	second continua emission bands are unstructured and very broad, order of 10 nm	 128 nm 150 nm 172 nm	systems pumped by intense electron beams	
ArF* KrF* XeCl		193 nm 249 nm 308 nm 100 ns up to 1 µs pulses	pulsed electrical discharges in laser tubes at 3 to 6 bar, 10 to 100 ns pulses	The three types cover 90% of market; repetition rates of 1 or 2 kHz

typically 3 cm diameter. Laser lines are selected by laser mirrors with wavelength dependent reflectivity. The total gain in a regular He–Ne laser tube is on the order of a few percent per pass. Reflectivity of one mirror is maximized (better than 99%), and the "output coupler" has a transmission of one or two percent. Typical light output power is a few milliwatts, and the overall efficiency of the device is between a per mill and a percent. Laser mirrors can be either mounted directly to the ends of the laser tube with bellows for alignment or as an external optical cavity. If the laser cell is closed by Brewster angle windows, the laser light will be linearly polarized, since Brewster windows have a low reflectivity and consequently a low loss only for one orientation of polarization. He–Ne lasers are used for alignment purposes and in metrology. Excellent spectral and spatial characteristics and stability has been achieved with helium–neon lasers, and it is still essentially the only compact, easy to use gas laser in the visible spectral range.

The great variety of collisional and radiative processes which can occur among many excited levels in neon or other rare gases leads to a great variety of laser lines [15, 16]. Some laser systems may operate continuously, others may lead to population inversion only for a short time interval following excitation by a pulsed discharge. Pulsed laser lines in neon (3p to 3s) have become important as model systems for very short wavelength lasers, often referred to as "X-ray lasers". Neon like ions are produced and excited by electron collisions in hot, laser induced plasmas [18]. With pulsed excitation there are two principle regimes for obtaining population inversion and laser effect, collisional excitation and recombination schemes. In the first case laser effect occurs during the pulse and in the latter in the afterglow by recombination processes.

Many ion laser lines can be observed in intense pulsed low pressure discharges. Triply ionized krypton at 176 nm delivers the shortest wavelength ion laser lines [14]. Soft X-ray wavelength emission was pioneered by Rocca and coworkers [19].

7.2.3 Ion Lasers

Ion lasers can also be operated in continuous mode. The best known ion laser systems use pure rare gases as the laser medium, argon in particular. In argon ion lasers singly ionized argon has the configuration $\ldots 3s^2p^5\ {}^2P^0_{1/2}$ and ${}^2P^0_{3/2}$. The two "ground state" levels differ in energy by only 0.18 eV. Inversion is built up because the lower 4s levels are more rapidly depleted than the upper 4p levels. The electron energy in the discharge has to be rather high for both ionization and excitation. The ionisation energy of argon is 15.759 eV and the 4p upper laser levels are again almost 20 eV above the ground state of the ion. Deviations from the quadratic increase of laser output with discharge current start above 600 A/cm^2 when formation of doubly charged ions sets in [14], p. 218.

Gas pressure and the diameter of the discharge tube of argon ion lasers are similar to those in He–Ne or other discharge pumped lasers operating on atomic transitions. Discharge currents, however, are about three orders of magnitude higher. Hot cathodes are used to provide high currents necessary for ion laser operation, and coaxial magnetic fields can improve laser performance. Ceramic tubes are used to handle

these high currents without too much sputtering. Active cooling by water or forced air has to be provided. The typical gain of ion laser lines is 1%/cm and the efficiency of the device is on the order of 0.1%. The discharge tubes are normally closed by Brewster angle windows and external optical resonators are installed. Many argon ion lasers provide the option of selecting the laser line by tuning an optical element such as a Littrow prism in the optical cavity. The argon ion laser with high output power and lines ranging from about 440 to 500 nm (near ultraviolet to green) is used to pump other lasers such as dye lasers. Finally, ion lasers are not limited to the use of rare gases as the active medium, but use metal vapors in rare gas buffer gases [15], p. 172.

7.2.4 Excimer Lasers

An interesting approach for obtaining population inversion in rare gases uses the fact that rare gas atoms can become chemically very reactive when they are not in their electronic ground state. This behaviour can be used to form molecules which exist only for a short period of time and then return to the ground state via radiative decay. The lower level of this radiative transition is instantly depleted since the species which formed the excited molecule are unbound in the ground state. Formation of the excited molecules, called "excimers" (an acronym for excited dimers), leads therefore automatically to population inversion, and lasers using this concept are known as excimer lasers. They were first demonstrated by Molchanov, Basov and coworkers in 1968 [20, 21] using electron beam excited rare gas crystals in which the excitation scheme is similar to dense gases. Excimer lasers in the gas phase were developed in the following years [22, 23]. Technical development of excimer lasers is still in progress. For basic concepts, see Charles Rhodes 1980 [24]. Excimer lasers which are widely used today are based on the formation of rare gas halide excimer molecules. From the possible combinations of He to Xe and F to I, the heavier rare gas with lighter halogen atoms show fluorescence and six combinations show laser effect [25]. The advantage of rare gas halide systems in comparison with pure rare gas excimers is their narrower emission line and the longer laser wavelength given above. Both features lead to reduced pumping power requirements.

The upper molecular level is populated via gas kinetic reactions, such as

$$Kr^* + F_2 \rightarrow KrF^* + F$$

and

$$Kr^+ + F^- + Ar \rightarrow KrF^* + Ar$$

with Ar used as a buffer gas. A general problem in excimer formation is to produce highly excited species like Kr^+ and Kr^* within a dense and rather cool gas in which molecules can form. Molecule formation can occur in the afterglow phase of a short, intense pulse of a high pressure glow discharge. Another technical difficulty in excimer laser design is to achieve a homogeneous excitation of the laser medium, since high pressure discharges tend to develop filamentation and arcing. Preionization of the laser gas with ultraviolet light is one solution of this problem. Excimer laser

transitions have lifetimes of a few nanoseconds and the electrically pumped lasers are operated using appropriate pulsed power circuits. In a short pulse regime 10 to 100 ns pulses are applied. Laser pulse duration is on the order of 10 ns in this case. In the so-called long pulse regime several 100 ns up to 1 μs pulses can be achieved. For a width of the discharge gap of 5 mm, 10 to 12 kV and, for a width of 15 mm, 25 to 30 kV are applied to drive the laser discharge. Discharge currents range from 0.1 to 1 kA. Repetition rates of 1 or 2 kHz are available from standard excimer lasers. High end devices for photolithography reach 4 kHz repetition rates with 30 to 40 W output power, time averaged.

A technical issue in the design of excimer laser tubes is to select materials which can resist the highly reactive halogen gases F_2 or Cl_2 and in particular the F and Cl radicals. Nickel and passivated aluminum are the preferred materials in excimer laser design. Other materials such as hydrocarbons have to be avoided.

Ceramic materials are used as insulators. Since the gas is chemically altered in the discharge channel, it has to be circulated in high repetition rate lasers to allow time for cooling and for the chemical components to return to their initial state, F_2 for example. A mechanical fan is used for that purpose. Its operation may contribute a significant fraction to the power consumption of the laser device. Laser tubes can provide typically 10^8 pulses before the gas has to be replaced, and 10^9 to several 10^9 pulses before the whole tube has to be at least overhauled by replacing the electrodes and optics. Optical gain per pass is very high during the short, tens of nanosecond pulses. Plane parallel resonators with a highly reflective back mirror and a highly transmissive (90%) output coupler are often used. The mirrors have to withstand an extremely high optical energy/power densities on the order of 100 mJ/cm^2 (10 ns pulses). A modern excimer laser tube is shown in Fig. 7.3. Excimer lasers have a wall plug efficiency of a few percent which is a high efficiency for short wavelength lasers.

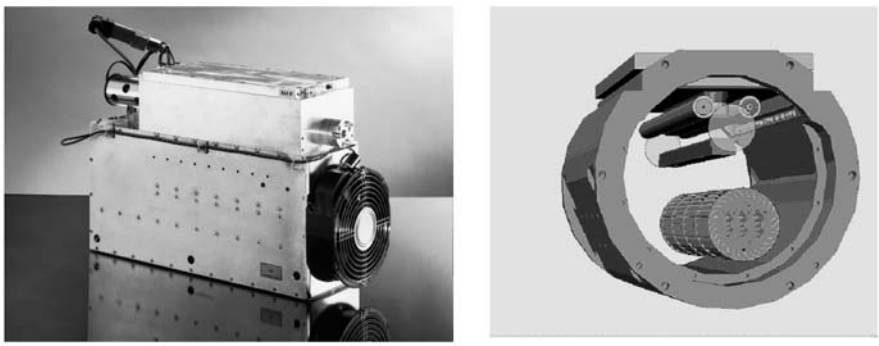

Fig. 7.3. Photograph of a compact, modern excimer laser (*left*). A cut through the laser tube is shown on the *right side*. The electrode configuration is shown in the *upper part* and the fan circulating the laser gas in the *lower part* of the drawing. Courtesy TuiLaser company, Munich, Germany

A present application which covers 70 to 80% of the market for excimer lasers is photolithography. There the lasers operate day and night with 5 to 10 mJ pulse power and 4 kHz repetition rate. The rest of the market is for micromechanics and medical applications, eye correction in particular. A number of 1000 to 10 000 shots are applied to each eye for that purpose.

7.2.5 Electron Beam Pumping of High Power KrF-laser

Because of their high efficiency, short wave length (248 nm) and high beam uniformity KrF-laser are presently the most attractive drivers for inertial fusion energy (IFE) [26]. To explore whether necessary laser beam power of several 100 TW and beam energy of several MJ can be generated with the required efficiency of more than 5% at affordable cost, programs have been started in several laboratories to develop the basic technologies [27].

High power KrF-lasers are pumped by large area high current pulsed electron beams. Because of their modularity, electron beam generators presently under development are considered to be scalable to the parameters required for a real IFE-driver. The main challenges are to develop a durable, efficient, and cost effective pulsed power system; a durable electron beam emitter; a long life, transparent pressure foil structure (that isolates the laser cell from the electron beam diode, the so-called hibachi); a recirculator to cool and quiet the laser gas between shots, and long life optical windows.

Typically, a single electron beam module must deliver 100 kA electron beam current with a particle energy around 500 keV to the laser cell for a duration of several 100 ns. Figure 7.4 shows a schematic of one half of the ELECTRA system presently constructed at NRL-Washington [27].

This system uses a capacitor/step-up transformer prime power system that pulse charges a pair of coaxial, water dielectric, pulse forming lines. The energy in the lines is then switched into the electron beam diode load using laser-triggered spark-gaps. A strong axial magnetic field is used to prevent pinching of the beam in the gas cell.

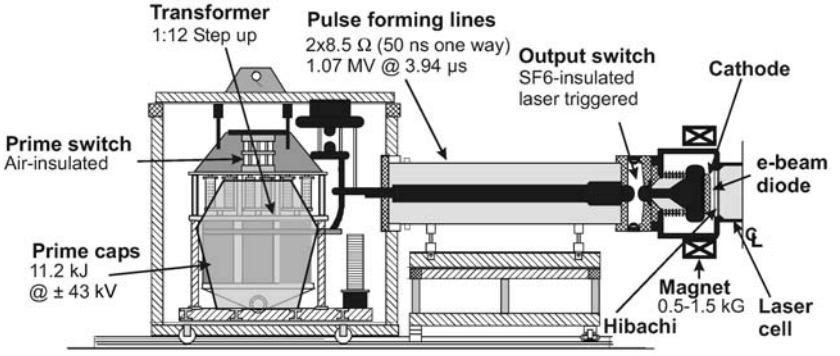

Fig. 7.4. One half of the ELECTRA pulsed power system: 500 kV, 100 kA, 100 ns flat-top electron beam, 5 Hz repetition capability

A general schematic of the diode, hibachi and gas cell is presented in Fig. 7.5. Besides the cathode, the hibachi foil support structure is the key element for a long-lived KrF-laser system. It must provide efficient and reliable electron beam injection into the gas. Plasma sources based on carbon fibres or metal dielectric structures look most promising as a durable electron source. To meet the high efficiencies required, the cathode emission must be restricted to areas between the ribs of the hibachi structure. In addition, the cathode emitter must be counter rotated by a fixed amount to compensate for the beam rotation in the axial magnetic guiding field.

Experiments have also shown that large area electron beams are subject to instabilities which can lead to energy spread and large divergence of the accelerated electrons [28]. To damp the RF oscillations, the cathode was built as a slow wave structure by loading the gaps between the segmented cathode areas with resistive elements. Long lifetimes (more than 10^8 pulses) of the hibachi foil are only possible if it is cooled efficiently. A recirculator used for that purpose does not only have to cool the foil and the laser gas but also has to quiet the gas before the next shot. A system based on louvers has been designed at NRL [29] to solve this task. It guides the gas stream towards the hibachi between shots and rapidly transfers the turbulent into a laminar flow during the pulse by opening the louvers.

Intense laser emission from electron-beam-pumped ternary mixtures of Ar, N_2, and POPOP vapor was investigated [30]. Powerful laser output was observed at 381 nm from electron-beam-pumped ternary mixtures of argon, nitrogen and 2,2′-p-phenylinebs<5-phenyloxazole (POPOP) dye vapor. The injection of the sub threshold 380.5 nm N_2-line into the electrically excited gain profile of POPOP vapor has been identified as a pumping mechanism.

The radiative energy transfer from the electron-beam-excited N_2 is apparently responsible for the excitation of the dye vapor.

The apparatus used consisted of a high-temperature high-pressure vapor cell with both electron-beam and optical access. The POPOP partial pressure in the cell was controlled by adjusting the temperature of the cell assembly with an oven enclosure. A prealigned plane-parallel optical resonator with high-reflectivity dielectric coat-

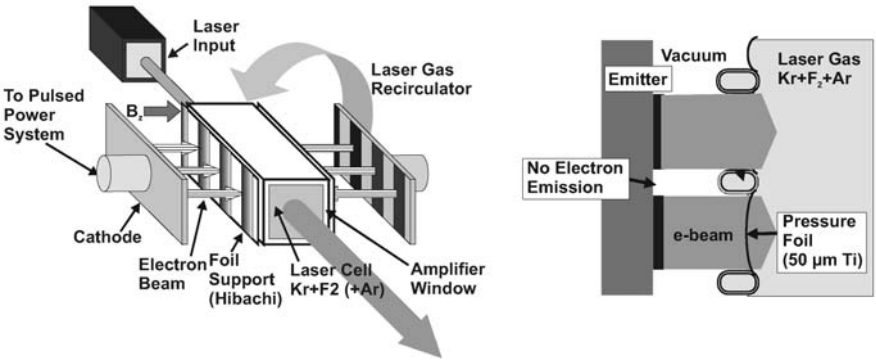

Fig. 7.5. Principal set-up of an electron beam pumped KrF-laser

ings ($R = 96\%$ at 385 ± 10 nm, $R = 70\%$ at 360 nm) was located inside the cell. The cell was isolated from the cathode of the electron-beam machine by a 0.075 mm thick titanium foil. This foil acted both as a pressure barrier and as the anode of the field-emission diode. A second 0.025 mm thick foil, located 0.3 cm away from the first one inside the cell, was used as a thermal barrier to prevent condensation of dye on the relatively cool anode foil. All experiments were performed on an S1 Apex I machine, configured for this experiment to produce a beam of 1-MeV electrons with a peak current of 28 kA in a triangular-shaped 30-nsec pulse, which corresponded to an input energy of 500 J. The output from the cell was measured with a spectrograph which had a 1 nm resolution. The output pulse was detected with a fast-vacuum photodiode and a Tektronix R7912 transient digitizer. Intense laser emission at 381 nm was observed in a 10 nsec pulse with less than 2 nm bandwidth and a 5 mrad beam divergence from an electron-beam-excited ternary mixture of 5 Torr POPOP, 2 atm Ar, and 4 atm N_2. Without optimization output power in excess of 500 kW was observed, indicating a conversion efficiency from deposited electronic energy into the active volume to optical output of at least 0.3%.

7.3 Smith–Purcell Effect

7.3.1 Historical Development

Tera-Hertz (THz) electromagnetic radiation is produced using an effect first explained by S.J. Smith and E.M. Purcell in 1953. The Smith–Purcell effect describes "Visible Light from Localized Surface Charges Moving Across a Grating". This effect occurs over a broad range of spectral wavelengths, including visible through millimetre wavelengths. The Smith–Purcell effect was the precursor of the free electron laser (FEL). Essentially, this is a form of Cherenkov radiation where the phase velocity of the light has been altered by the periodic grating [31].

7.3.2 Electrophysical Fundamentals

The electron charge of the beam induces an image charge in the metal grating. Due to the mechanical geometry of the grating bars and groves, this image charge oscillates and this generates an electromagnetic field as a standing wave above the grating. Since the electron is fast, this wave is coherent along the grating. The observed wavelength of the emitted light depends on the grating period D and the observation angle Θ with respect to the velocity vector of the electrons. This is given by

$$\lambda = D(\beta^{-1} - \cos\Theta), \tag{7.12}$$

where β is v/c, i.e. the electron velocity divided by the speed of light.

7.3.3 Present State

A strictly analytical approach explaining the Smith–Purcell effect is given by di Francia [32]. FEL systems were constructed by Walsh and his group using a conventional SEM setup [33]. The "Tabletop"-SEM FEL setup of Vermont Photonics shines an intense electron beam parallel to a mechanical grating of mm pitch. Changing the electron beam voltage allows continuous tuning of the THz output wavelength from 100 μm to 1 mm wavelength.

Present solutions for the problem are huge electron accelerators [34]. Presently worldwide 30 FEL installations using very high electron energies are installed, 10 are in development and further 10 are planned. However, the available beam time and lines number is not sufficient to exploit many applications of THz radiation. The most prominent characteristics of FEL are as follows.

Tunability by voltage and grating change. Using an undulator, a factor-of-10 tunable frequency range has already been demonstrated with the same accelerator, see Fig. 7.6. High peak power, since waste energy is carried away at nearly the speed of light and the lasing medium cannot be damaged by high optical fields. FELs can produce very high peak powers; gigawatt peak powers have been demonstrated. Flexible pulse structure using mature RF technology of linear accelerators to manipulate and control the FEL pulse structure. Picosecond pulses with sub-picosecond jitter can be produced at a rate of 10/sec. FELs have a good laser characteristics achieved by a single transverse mode, high spatial and temporal coherence, and flexible polarization properties.

Because the gain medium is transparent at all wavelengths, FELs in principle can produce radiation at any wavelength. In practice, electron beam energy, current, emittance, and energy spread requirements become more stringent as the wavelength decreases, and the cost, size, and complexity of the FEL are therefore higher at shorter

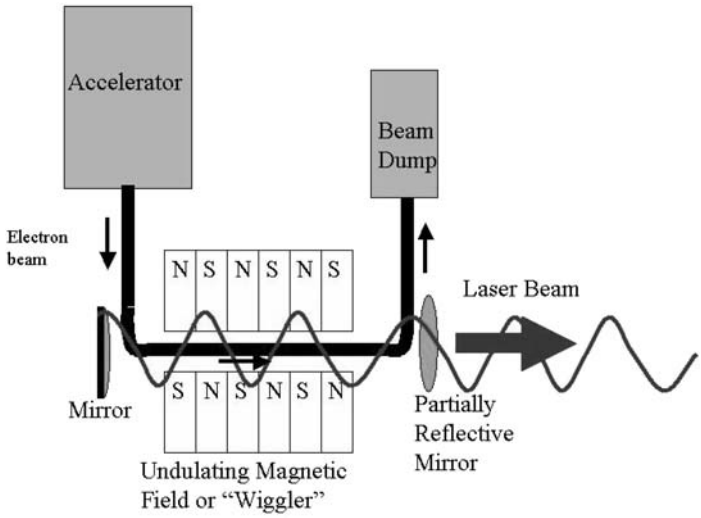

Fig. 7.6. Schematic of a FEL installation in nuclear physics or national institute

wavelengths. FELs can have significant emission at harmonics of the fundamental frequency given by the resonance condition. The shortest wavelength achieved so far in an FEL is 240 nm. FELs for scientific research have been restricted to the infrared region. Now, there are proposals to build vacuum ultraviolet and X-ray FELs. Size and cost of present FEL's used principally in central facilities are huge. Tabletop and portable powerful solutions are needed in the scientific and technical community.

7.3.4 Future Aspects for THZ Sources

Recent workshops require the development of a portable or small source for various applications. One approach is to employ a modified SEMs, as described by Walsh et al. [35, 36]. The power of the emitted light from a SP device can be calculated depending on the assumed beam shape with different formulas, which describe the linear power-gain regime [37, 38]. When achieving 1 to 218 μA currents in the beam, the exponential gain regime for the emission power is reached [39–41]. The wavelength regime from 8 μm to 1,400 mm can be covered with electron beam energies below 1000 eV. Tuning the electron energy, even X-ray generation is possible. The X-ray FEL is still under investigation since efficient S-P X-ray generation requires relativistic e-beams having a transverse momentum and dimension whose product approaches the Heisenberg uncertainty limit [42].

7.4 Millimetre and Infrared Light Sources

7.4.1 Historical Development

Millimetre and infrared light, and tera-hertz waves (THz) are electro-magnetic waves and cover a wavelength regime of 100 mm to 1 μm. Figure 7.7 gives a schematic of the dimensions of wavelength, frequency and energy for those radiations.

The propagation is governed by Maxwells equations. The interaction with matter is correlated to the weak energy of THz photons. Diffraction and/or guiding properties of devices in the THz regime are linked to the sub-mm THz wavelength, also called far infrared (FIR). Due to the period of THz waves in the picosecond regime, ultra-fast phenomena in matter can be investigated. Measurements use the time domain spectroscopy.

Infrared radiation is electromagnetic radiation having a wavelength in the range 0.000075–0.1 cm. Infrared rays thus occupy that part of the electromagnetic spectrum with a frequency less than that of visible light and greater than that of most radio waves, although there is some overlap. Infrared radiation is thermal (or heat) radiation. It was first discovered in 1800 by Sir William Herschel, who was attempting to determine the part of the visible spectrum with the minimum associated heat in connection with astronomical observations he was making. In 1847, A.H.L. Fizeau and J.B.L. Foucault showed that infrared radiation has the same properties as visible light, being reflected, refracted, and capable of forming an interference pattern. Infrared radiation is typically produced by objects whose temperature is above 10 K [43].

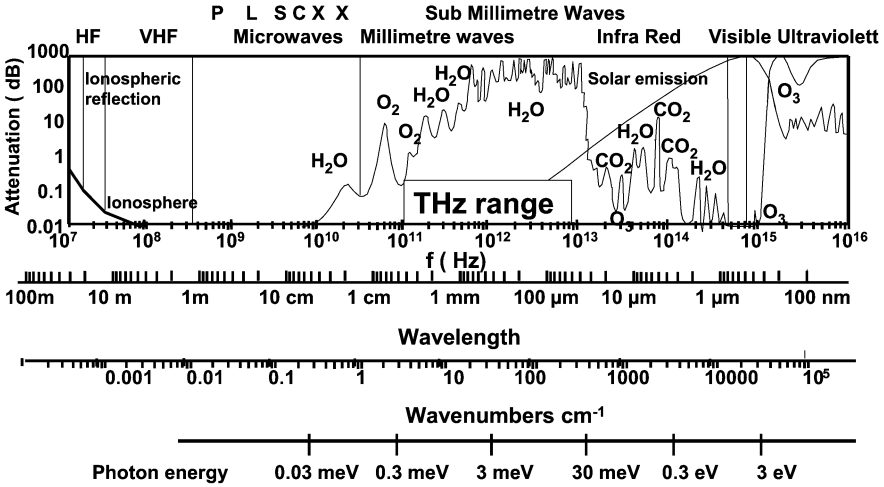

Fig. 7.7. Ranges of wavelength, frequency and energy for mm, THz, and IR radiations. Also, the attenuation in dB/km is given versus the wavelength

7.4.2 Generation of IR Radiation

Visible light is emitted from sources with a temperature of above 1900 K, as a candle does. The temperature of a human body emits radiation with a wavelength of 8 µm to 9 µm and can be observed only with an IR detecting camera or sensor. Typically, all hot surfaces emit IR radiation. Intensive IR lamps are incandescent lamps, which are generally used with a special filter to block out the visible spectrum.

7.4.3 IR Applications

There are many applications of infrared radiation. A number of these are analogous to similar uses of visible light. Thus, the spectrum of a substance in the infrared range can be used in chemical analysis. Radiation at discrete wavelengths in the infrared range is a characteristic of many molecules. The temperature of a distant object can also be determined by analysis of the infrared radiation from the object. Radiometers operating in the infrared range serve as the basis for many instruments, including heat-seeking devices in missiles and devices for spotting and photographing persons and objects in the dark or in fog [44]. Medical uses of infrared radiation range from the simple heat lamp to the technique of thermal imaging, or thermography. A thermograph of a person can show areas of the body where the temperature is much higher or lower than normal, thus indicating some medical problem. Thermography has also been used in industry and other applications. The higher sensitivity of longer-wavelength allows doctors to detect tumors using thermography, or heat analysis. It allows pilots to make better landings with improved night vision, and environmental scientists to monitor pollution and weather patterns [45]. Thermal

Fig. 7.8. *Left*: black and white image of a man's head in visible light, *left*, and the IR image, *right*. *Right*: airplane after takeoff with clearly shown jets and also hot tires of the wheels

insulation survey of buildings is performed. Other possible uses include law enforcement, search and rescue, and industrial process control [46].

In quantum detectors the THz photon excites an electron from a filled state into an empty state, for example, between an impurity state and the conduction band in a semiconductor (Ge:Ga, InSb, etc.) [47]. The sensitivity of such detectors is high: 10^{-12}–10^{-13} W/%Hz at 0.3 to 5 THz; however, they need cooling to a very low temperature (4 K or less), which is obtained by very small Stirling coolers, now commercially obtainable [48].

Figure 7.8 shows (left) the black and white image of a man's head in visible light, left, and the IR image, right. The photo on the right shows an airplane after takeoff with clearly shown jets and also hot tires of the wheels. A new infrared video camera with Infrared Focal Plane Array Technology uses quantum-well infrared photodetectors. The array is designed to detect infrared radiation of 8- to 10-μm wavelength. The camera is capable of detecting a temperature difference of 0.01°C.

7.4.4 Generation of THZ Radiation

The shortest wavelength achieved so far in an FEL is 240 nm. FELs for scientific research have been restricted to the infrared region. Now, there are proposals to build vacuum ultraviolet and X-ray FELs. Size and cost of present FEL's used principally in central facilities are huge. Tabletop and portable powerful solutions are needed in the scientific and technical community.

7.4.5 THz Applications

Applications are in the fields of spectroscopy and imaging. Radio astronomy employs remote space observatories in the FIR and THz regime with super-conducting detectors, cold mirrors and m^2 collecting aperture. Terahertz devices peer through paper and clothing, revealing concealed weapons and explosives.

Molecular vibrations in solids are used to measure spectroscopic fingerprints of molecules and compounds [49]. In biology especially unstained DNA analysis is the goal and theoretically predicted as a possibility [50]. Also, binding states can be detected and analysed. Also, single base mutations in chromosomes can be detected and help to distinguish inherited diseases. Medical applications are: tissue analysis [51], especially for cancer diagnostics in pathology [52], medical treatments without radiation damage of the surrounding tissue, imaging of human tooth for caries detection.

Other important applications are in defence and security, observation of status of materials, e.g. cracks in the foam insulation of the American space shuttles, detection of explosives and detonation chemicals, detection and analysis of drugs, screening of passengers for hidden metals, short range communications in combat, biological and chemical agent detection, toxic and chemical mapping and identification after bomb explosion.

Environment and materials applications to investigate surfaces and interfaces with THz dark field radar [53]. THZ radiation using eV to meV photons only warm up the samples a little, since the total output power of today's sources ranges in average 0.1 to 100 W DC. So far the technology lacks a portable and bright in a wide range tuneable THz-radiation source. Military and research agencies offer big money for a solution.

The analysis is simplified by a high chemical specificity. To characterize special compounds, an internationally accessible library of THz spectral signatures has to be built up. The fingerprint spectra of the compound contain rotational lines (gas); phonon bands (crystal); large amplitude collective modes (macromolecules). The presence of spectral signatures leads to non-subjective algorithms. The frequency regime for the THz fingerprint of matter is given in Fig. 7.9

For analysing the mechanical roughness of surfaces, a THz radiation source capable of emitting 300 μm radiation is sufficient and can image roughness above this wavelength, since the imaging system cannot see all the scattered noise from objects of the size of shorter wavelength.

THz screening is non-invasive, non-destructive, non-detectable, since THz is non-ionising. Very low power levels $\ll 1\ \mathrm{mW/cm^2}$ are for sensing are required. Many common, non-metallic container, shipping, and clothing materials have sufficient transmission for spectroscopy of their contents. Investigations have identified strong spectral features and fingerprints of explosives and drugs.

Preferred applications are: automated threat detection and personnel screening, molecular analysis of tissue, chemicals and fast screening of reactions without the need of a tracer or fluorescent addition to the reacting molecules.

Today one observes a rapid roll-off of the performance of electronic devices above 100 GHz. New more powerful sources are developed. For THz-radiation generation mostly negative differential conductance devices and transit time limited devices are employed, e.g. Gunn diodes, avalanche and transit time devices like Impatt diodes, and superlattice devices which use Bloch oscillations in a miniband and transit time limitation in the active region. Semiconductor heterostructure engineering with bandgap-, eigenstates-, and carrier-lifetime engineering are developed. Transis-

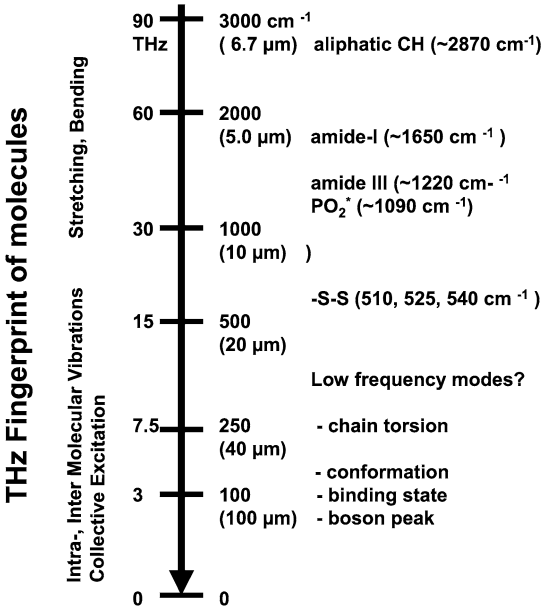

Fig. 7.9. Frequency regime for the THz fingerprint of matter with examples

tors with high mobility 2D electron gas n(HFET's) [54, 55], as well as transistors called n(HFET).

Quantum cascade lasers [56] generate THz radiation in the wavelength region 3.5 to 160 µm in pulse mode at RT and continuous mode at 77 K with tens of mW output power. Operation at room temperature is the challenge. Inter-subband transitions are used and the cascade scheme, where more phonons per electron are generated. A narrow linewidth of 4.6 THz is obtained.

Resonant tunnelling diodes are a low power source at 712 GHz, also Heterostructure Barrier Varactors.

Photomixing is employed for emitters and detectors. Powerful sources are miniaturized synchrotrons and beam transmission lines. The classic sources for THz-radiation generation are the large synchrotron and accelerator facilities which employ wigglers and Smith–Purcell grating sources and deliver mW to W output intensity. Those institutions presently offer their beam and experimental facility locations for measurements at a rate in the range of 1000 US$ per day to companies and research organisations.

7.4.6 Further Developments

To make THz spectroscopy, analysis and imaging a viable technology, however, a portable source is needed. Presently photonic sources are femto-second-laser based systems at cost 100–150 k$. Continuous wave diode laser sources cost half of this.

Wanted is a cheaper, more compact source, e.g. sub-GHz by a microelectronic approach, but will it be cheaper? Are quantum cascade lasers a solution?

7.4.7 Detection of THz Radiation

Several different detectors are in use: terahertz materials-metamaterials with negative refractive index and negative permittivity [57] and photonic bandgap materials. Others are: antenna-amplifier arrays, bolometers and optical 2 wave mixing for generation of photoconductivity in semiconductors, or using single electron transistors as detectors [58]. Those allow to detect 10^{-17} W/sqrt Hz at 500 GHz but at 70 mK.

7.5 Visible Light Sources

7.5.1 History and Introduction

The development of electrical visible light sources started with the invention and production of the incandescent lamps in 1880. Major improvements have been achieved over the past decades with respect to lamp efficiency, lifetime and colour properties, see Fig. 7.10. Further aspects like miniaturization and environmental aspects are some of the market drivers for the development of new and innovative products.

Incandescent lamps deliver thermal emission of radiation close to thermal equilibrium, low and high-pressure discharge lamps yield atomic and molecular emission from gas discharges, and LEDs emit light from solid state diodes. The latter type will not be addressed in this paper.

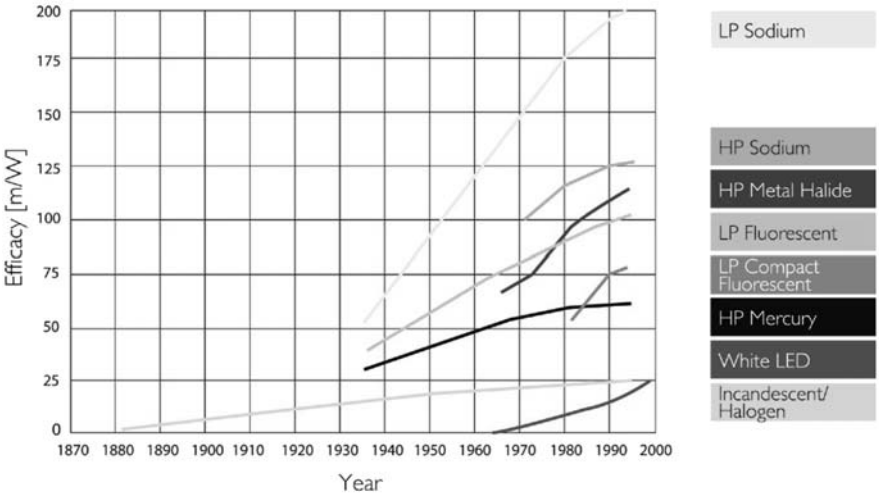

Fig. 7.10. Temporal development of luminous efficiencies of electrical light sources

7.5.2 Incandescent Lamps

The incandescent lamp is the oldest electrical light source with the largest market segment of about 11 billion pieces world-wide. It is used especially where small lumen packages are needed and where simple, cheap and compact lighting solutions are preferred [59].

Normal Incandescent Lamps

In incandescent lamps photons are produced by the electrical heating of a metal wire. Its high temperature results in radiation emission in the visible part of the spectrum.

According to Planck's law, the filament of an incandescent lamp must be heated up to at least 2400 K for production of a white emission spectrum. The metal wire is mounted in a glass bulb filled with an inert gas, as indicated in Fig. 7.11. Higher filament temperatures could render more efficient conversion of electrical energy into visible light, but would reduce lamp life due to enhanced metal evaporation. For this reason, the filaments of incandescent lamps are made of tungsten having a high melting point and a low vapor pressure. Lamp lifetime can be further improved by the reduction of the tungsten evaporation rate when adding rare gases such as krypton or xenon. Halogens are used for realizing a regenerative cycle in order to effectively transport back tungsten to the filament.

In normal incandescent lamps tungsten evaporates off the filament and condenses on the bulb wall, resulting in a reduced lumen output over lamp life. This is reduced when iodine, bromine or chlorine is added to the gas filling. The halogens are forming volatile tungsten compounds at the glass wall being transported back to the hot filament where the tungsten halides are decomposed again, see Fig. 7.11 right side. As a result of lowering the net evaporation rate of tungsten, the filament of halogen lamps can be operated at higher temperature as compared to standard incandescent

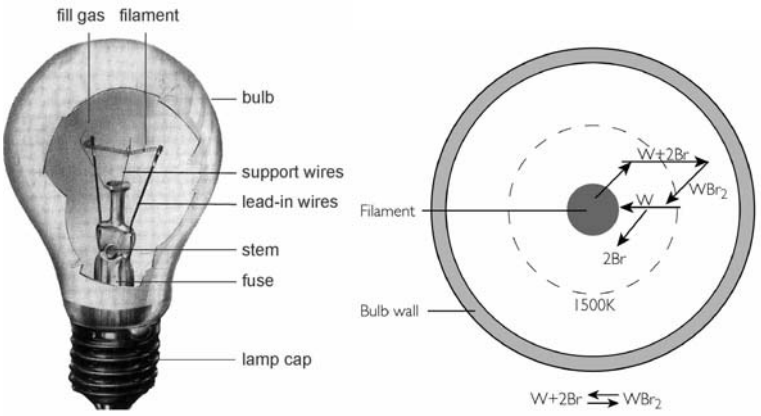

Fig. 7.11. *Left*: schematic drawing of an incandescent lamp. *Right*: schematic of chemical transport cycle in tungsten halogen lamps

lamps. Consequently, luminous efficiencies can be increased at reduced lamp size, which is relevant for applications in compact reflectors.

7.5.3 Gas Discharge Lamps

A gaseous discharge (plasma) is obtained by driving an electric current between two adjacent electrodes through a partially ionized gas enclosed in a discharge tube, typically made of quartz. Also, pulsed discharges with a dielectric barrier between the electrodes and the plasma are used for plasma display applications. Also, electrodeless microwave excited discharges can be used as light sources.

Many physical factors influence the electrical and light technical properties of a gas discharge, such as the type and pressure of the gas, electrode material, operating temperature of the electrodes, shape and surface structure of the electrodes, electrode distance, geometry of the discharge vessel, and current density. For the purpose of light generation, two basic types are distinguished: low-pressure and high-pressure discharge lamps. For lighting applications, both are operated in the arc discharge mode, which is characterized by high current densities, more than 1 A/cm^2. Electric currents are limited by using inductances or electronic ballasts [60].

In low-pressure discharge lamps, the gas pressure is typically less than 100 Pa. Consequently, the mean free path length of electrons is larger or in the order of the discharge tube diameter, e.g. a few cm. Under these conditions, they gain high energies of more than 1 eV from the applied electric field due to low collision rates with the neutral gas atoms. Finally, the cold atoms are effectively excited by inelastic collisions with the hot electrons. The temperature difference of electrons and atoms reflects the situation of non-thermal equilibrium, as shown in Fig. 7.12.

In high-pressure discharge lamps the operating pressure is typically in the range between 10 kPa and 10 MPa. Under these conditions, collisions between electrons and atoms or ions are much more frequent, and a local thermal equilibrium (LTE) with close by or equal particle temperatures is established.

In low-pressure gas discharge lamps, atomic line radiation is emitted preferably from resonance transitions of the element with the lowest excitation potential.

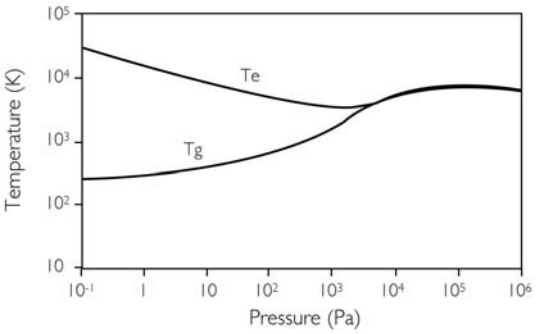

Fig. 7.12. Temperatures of electrons and neutral gas as a function of gas pressure

For mercury these transitions are in the deep UV wavelength region at 185 nm and 254 nm, whereas from sodium visible radiation at 589 nm is emitted.

In high-pressure discharge lamps various contributions to the spectrum are obtained: spectrally broadened atomic lines (resonance-, Van der Waals- and Stark-broadening), molecular radiation bands and quasi-continuous emission due to free-free (Bremsstrahlung) and free-bound (recombination of electrons with ions and atoms) transitions. As a result, the colour rendering properties of high-pressure discharge lamps are fair to excellent, depending on the type of filling [61].

Review of Gas Discharge Lamps

Table 7.2 gives a review of the most relevant types of gas discharge lamps. The light sources differ with respect to the emission spectra and application fields. Luminescent materials are applied for conversion of UV-radiation into visible light for low-pressure mercury, sodium and xenon excimer lamps.

Low-Pressure Mercury Lamps

In Fig. 7.13 the working principle of a low-pressure mercury lamp (also known as fluorescent lamp) is shown. They are designed in the form of a linear or bended tubular bulb with the electrodes sealed in at the end parts. Also, electrodeless lamps are available, where the electrical energy is coupled inductively into the discharge vessel via externally mounted metal coils. A rare gas, e.g. argon, is filled as starting gas in addition to a few mg of mercury. At low pressures in the order of a few pascals, about 97% of the emission from Hg atoms is in the ultraviolet wavelength region. Therefore, the inner surface of the bulb is coated with a fluorescent powder (phosphor), which efficiently converts the UV radiation into visible light. The composition of the phosphor materials determines the spectral power distribution and colour of emitted wavelengths.

Table 7.2. Review of basic types of gas discharge lamps

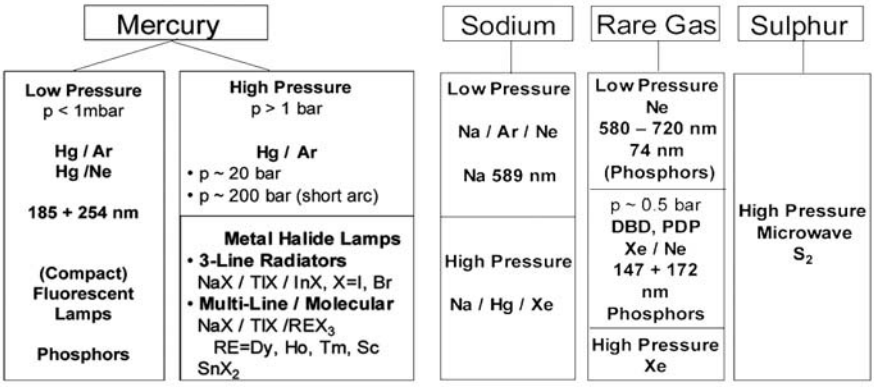

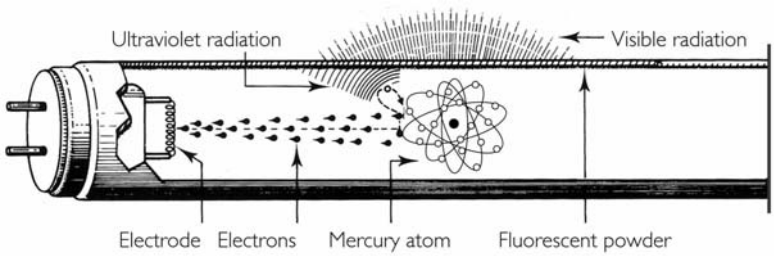

Fig. 7.13. Schematic of a low-pressure mercury discharge (fluorescent) lamp

The generation of UV photons arises from transitions of mercury atoms between the excited state levels $^1P_1$, $^3P_1$ and the ground state level $^1S_0$. About 64% of the electrical input power is converted into UV photons at a wavelength of 185 nm and 254 nm. Only 3% are directly emitted as visible light (405 nm, 436 nm, 546 nm and 589 nm). Although the quantum efficiencies of applied phosphors are close to unity, i.e. one UV photon is converted into one visible photon, the overall efficiency for visible radiation is only 28% due to the large Stokes shift. This value corresponds to a luminous efficiency of about 100 lm/W.

Typical ranges of fluorescent lamp parameters are: electrical input power up to 140 W, luminous efficiency up to 100 lm/W, colour temperature between 2700 K and 8000 K. The lamps are available in various geometries, e.g. cylindrical, circular or U-shaped tubes. The latter are also known as energy saving or compact fluorescent lamps. Depending on lamp construction, lifetime ranges from 5000 to 25 000 hours.

7.5.4 Fluorescent Coatings

The fluorescent powder or phosphor is an essential part of a fluorescent lamp since it is designed to obtain the required visible radiation. It is coated onto the inner side of the glass tube in order to effectively absorb UV photons from the discharge. The powder consists of one or several luminescent materials, which are in general inorganic compounds doped by transition metals (e.g. Mn^{2+}, Mn^{4+}) or rare-earth ions (e.g. Tb^{3+}, Eu^{3+}). The composition of the fluorescent powder is optimized for an efficient absorption of the atomic resonance lines of mercury. In addition, it efficiently emits photons in the required visible spectrum. In some cases the fluorescent composition also consists of a so-called sensitizers (e.g. Ce^{3+}). It is used if the first dopant (the activator) does not sufficiently absorb the UV radiation of mercury. The light conversion process begins with the absorption of incident photons either by the activator or the sensitiser. In the latter case, the energy is subsequently transferred to the activator. The excited activator ion, for instance Eu^{3+}, decays to the ground state by emitting a photon. Its wavelength corresponds to the energy gap between the excited and ground state. The energy difference between the emitted and the absorbed photon represents the Stokes shift. This energy loss of about 50% is dissipated as heat in the fluorescent powder.

Table 7.3. Review of most commonly used luminescent materials in fluorescent lamps

Composition of luminescent materials	Emitted peak wavelength (nm)	Color point x, y[a] (after CIE 1931)	Example of application area
LaB_3O_6:Bi,Gd	311	–	medical lamps
$LaPO_4$:Ce	320	–	tanning lamps
$BaSi_2O_5$:Pb	350	–	tanning lamps
SrB_4O_7:Eu	368	–	black light lamps
$Sr_2P_2O_7$:Eu	420	0.167, 0.014	reprography lamps
$BaMgAl_{10}O_{17}$:Eu	453	0.150, 0.070	colour 80 lamps[b]
Zn_2SiO_4:Mn	530	0.256, 0.700	decoration lamps
$LaPO_4$:Ce,Tb	543	0.343, 0.585	colour 80 lamps[a]
$CeMgAl_{11}O_{19}$:Tb	543	0.350, 0.582	colour 80 lamps[a]
$GdMgB_5O_{10}$:Ce,Tb	543	0.346, 0.531	colour 80 lamps[a]
$Y_3Al_5O_{12}$:Ce	560	0.453, 0.523	colour 90 lamps[a]
$Ca_5(PO_4)_3$(F,Cl):Sb, Mn	575	0.356, 0.377	halophosphate lamps
Y_2O_3:Eu	611	0.643, 0.344	colour 80 lamps[a]
$GdMgB_5O_{10}$:Ce,Tb, Mn	630	0.602, 0.382	colour 90 lamps[a]
$Mg_4GeO_{5,5}F$:Mn	660	0.700, 0.287	decoration lamps

[a] At 254 nm excitation
[b] See text

Today, fluorescent materials compositions with quantum efficiency close to unity are commercially available. Table 7.3 gives a review of most commonly used phosphors, their characteristics and examples of application areas. For illumination purposes, halophosphate phosphors are still favoured. They yield a white emission spectrum with a reasonable efficiency and colour rendering. However, a trichromatic phosphor blend results in improved lamp efficiency and better colour rendition. An ordinary phosphor blend comprises $BaMgAl_{10}O_{17}$:Eu, $LaPO_4$:CeTb, and Y_2O_3:Eu. In Table 7.3 such so-called colour 80 lamps are indicated with an asterisk. They exhibit a spectral power distribution as shown in Fig. 7.14.

A further improvement of color rendition is obtained by using a tetra- or pentachromatic phosphor blend. Colour 90 lamps additionally consist of phosphors with an emission band position where the trichromatic phosphor blend does not radiate, viz. in the yellow ($Y_3Al_5O_{12}$:Ce) and deep red ($GdMgB_5O_{10}$:Ce,Tb,Mn) part of the spectrum.

Today, the tuneability of fluorescent lamp spectra results in many other application areas beyond illumination, such as medical and cosmetic skin treatment, decoration, reprography and horticultural lighting. The latter, for instance, comprises a dichromatic phosphor blend consisting of $BaMgAl_{10}O_{17}$:Eu and Y_2O_3:Eu. Its emission spectrum is optimised with respect to the action spectrum for photosynthesis of green plants.

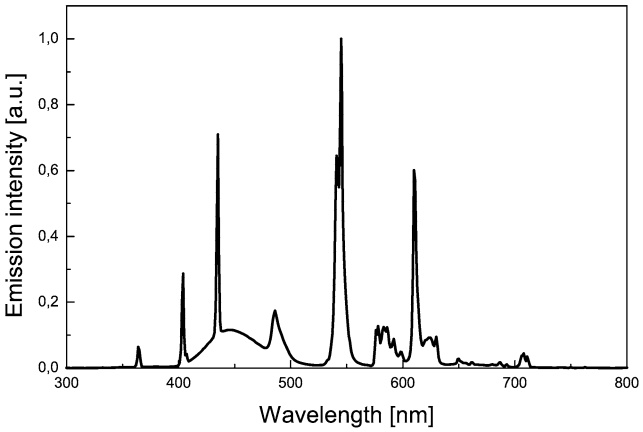

Fig. 7.14. Spectrum of colour 80 fluorescent lamp comprising a blend out of $BaMgAl_{10}O_{17}$:Eu, $LaPO_4$:Ce,Tb, and Y_2O_3:Eu

Other Low-Pressure Discharge Lamps

The main difference of low-pressure sodium lamps to mercury lamps is given by the fact that sodium significantly emits radiation directly in the visible spectrum. The Na D-lines deliver almost monochromatic yellow light from the doublet at 589.0 nm and 589.6 nm. Furthermore, the melting point of Na is higher compared to Hg resulting in an optimal operating temperature of about 530 K. At these temperatures the Na metal is highly reactive. Therefore, a chemically stable wall material like quartz (SiO_2) or alumina (Al_2O_3) is required. As indicated in Fig. 7.15, thermal losses are reduced by mounting the discharge tube inside an evacuated outer bulb.

Due to the low excitation energies and convenient spectral position of the Na D-lines, these lamps exhibit the highest ever achieved luminous efficiency. At a discharge power of 200 W values of 200 lm/W at an overall system efficiency of 172 lm/W are realized. Unfortunately, a low rendition of colours is obtained due to missing emission at other wavelengths, e.g. in the blue, green and red part of the spectrum. For this reason the application of low-pressure sodium lamps is limited mainly to street and outdoor lighting where high efficiencies and long lifetime of about 20 000 hours are required. The poor colour rendition can be further improved by increasing the sodium vapor pressure to atmospheric values. In high-pressure sodium lamps, the Na D-lines are spectrally broadened, as described in the section below.

Besides low-pressure mercury and sodium lamps also other types of radiators such as neon and xenon are known. For example, low-pressure neon lamps are applied in automotive brake lights and advertisement lighting. Excimer UV-radiation from xenon is used in plasma displays and flat backlights, photocopier lamps and UV-purification devices. Here, atomic and molecular radiation of xenon at 147 nm and 172 nm is emitted, respectively. A major advantage of these discharges is their

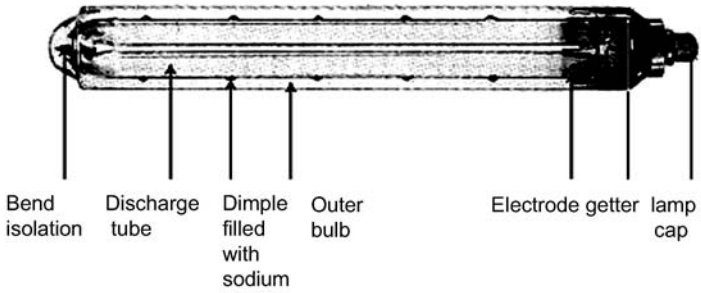

Fig. 7.15. Build up of a low-pressure sodium lamp

fast switching behaviour since in contrast to mercury and sodium, xenon is already in the vapor state.

7.5.5 High-Pressure Discharge Lamps

When raising the pressure in a low-pressure discharge, the rate of elastic collisions increases. Although each collision transfers only little energy to heavy particles, the plasma is heated effectively due to large particle densities. As a result, a plasma temperature gradient establishes in order to sustain central plasma temperatures in the range between 4000 and 10 000 K. The heat flux along the temperature gradient to the discharge wall represents a thermal loss of energy limiting the radiation efficiency to around 60%. Selective emission of the plasma arc is used for efficient visible radiation. High-pressure discharge lamps contain metals like mercury or sodium.

In the so-called metal halide lamps also other efficient radiators are added to the lamp filling. Different combinations of metals generate visible radiation with various colours and radiant efficiencies. Theoretically, at least, no fewer than 50 different metals, typically dosed in the form of metal halide compounds, can be used as additives. Lamp manufacturers have introduced various combinations on the market with a wide range of applications.

In high-pressure sodium and metal halide lamps a major technical breakthrough has been realized by the introduction of polycrystalline alumina (PCA) – a sintered Al_2O_3 ceramic – as a wall material. Compared to quartz, it is much more chemical resistant against hot sodium vapor. Therefore, PCA is used as a wall material in high-pressure sodium lamps. Generally, ceramic materials allow lamp operation at high wall temperatures resulting in an effective evaporation of the salt fillings. In contrast, lamps with quartz envelopes are limited to maximum wall temperatures of about 1370 K due to re-crystallization effects. However, the design of PCA lamps and vacuum tight sealing of electrodes is more complicated as compared to quartz due to inconvenient thermal expansion behaviour and brittleness.

High-Pressure Mercury Lamps

In Fig. 7.16 (left) the construction of a high-pressure mercury lamp is illustrated. The discharge tube is filled with mercury and argon as a starting gas. The discharge vessel is mounted in an evacuated outer bulb in order to reduce thermal losses. Ignition of the plasma is realized by applying a high voltage pulse in the order of several kV. After ignition, the plasma enters the arc regime which is characterized by a low operating voltage (about 20 V) and high discharge current (>1 A). At this stage, the lamp is mainly emitting UV radiation from mercury at 254 nm and some light from the starting gas. As a result of thermal losses from the plasma, wall temperature increases with time causing enhanced evaporation of the liquid mercury. With a further increase in mercury vapor pressure, the radiated energy is concentrated progressively towards spectral lines of longer wavelengths since higher lying energy levels are excited. The run-up of the lamp enters a steady-state phase when a mercury pressure of typically 200–1000 kPa is established. Even at these pressures, part of the emission is in the UV region which can be converted into visible light by coating the inner surface of the outer bulb with a fluorescent powder, e.g. YVO_4:Eu. Besides efficiency, also colour rendering is improved significantly.

In high-pressure discharge lamps, mercury is introduced also as a so-called buffer gas resulting in elastically scattering of electrons by mercury atoms. By this mechanism, a low electrical conductivity of the plasma is adjusted. According to Ohm's law, electrical field strengths on the order of several 10 V/mm are present in the discharge column. Typically, lamp voltages in the range of 60–90 V are needed since at a given electrical input power only moderate discharge currents can be tolerated over lamp life. Electrode temperatures are in the range between 2400 and 3500 K, the

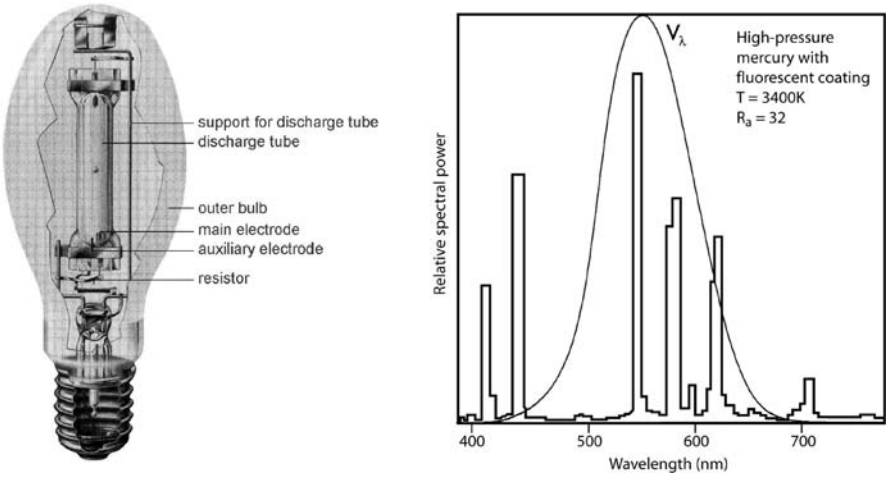

Fig. 7.16. *Left*: construction of a high-pressure mercury lamp. The inner surface of the outer bulb may be coated with a phosphor additionally converting UV radiation into visible light. *Right*: spectrum of a high-pressure mercury lamp

electrons being generated thermionically. For mercury both properties – its volatile character enabling large atom densities and its large cross-section for elastic electron scattering – are unique. Unfortunately, mercury is an environmental hazard and the lighting industry aims for the realization of mercury-free products in the near future [59].

High-pressure mercury lamps are used in various indoor and outdoor applications. The power ranges from 50 up to 1000 W with luminous efficiencies around 50–60 lm/W. Colour rendition is only moderate to poor. Colour temperatures range from 3400 to 6000 K.

A recent development of a high-pressure mercury discharge is the UHP lamp, which was invented by PHILIPS in the 1990s. This lamp has a very high operating mercury pressure (about 2×10^7 Pa) and a short arc length of about 1 mm only. This point-like white light source is applied in TV projection systems and beamers. In contrast to conventional high-pressure mercury lamps, a significant part of the visible radiation is generated not only by pressure broadened atomic mercury lines but also by Hg_2 molecules. UHP lamps are available on the market in the power range between 100 and 250 W. One of the key issues of UHP lamps is to maintain stable properties of the plasma and electrodes for several thousands of hours. As lined out in the next section, this can be achieved by adjusting a so-called regenerative chemical cycle: evaporated tungsten is transported back onto the electrodes via compounds including oxygen and bromine. Furthermore, UHP lamps have to be operated with special electronic devices in order to control electrode erosion and arc jumping.

Metal Halide Discharge Lamps

The construction of metal halide lamps is quite similar to high-pressure mercury lamps. Besides mercury and argon, metal halides are added to the lamp fill. Large particle densities are needed for efficient radiation emission in the visible spectrum. Metal halides are also less aggressive with respect to wall corrosion as compared to the pure metals.

Three main groups of metal halide lamps are distinguished: multi-line radiators, molecular radiators and three-band colour radiators. In the first type rare-earth halides like DyX_3, HoX_3, TmX_3 or ScX_3 (X = I, Br) are added to the lamp filling. These species have a large number of transitions at low mean excitation energy. Such plasmas efficiently emit multi-line radiation in the visible spectrum. Typically, NaI and TlI are added to such lamp fillings to improve luminous efficiency and colour properties. The second type is based on molecular radiators like SnI_2 or $SnCl_2$, which produce a quasi-continuous spectrum. The third class comprises mixtures of NaI, TlI and InI_3. The resulting spectra consist of three colour bands in the yellow, green and blue, respectively.

In Fig. 7.17 the spectra of these basic lamp types are shown. Application areas are found for various indoor and outdoor lighting purposes. The electrical input power ranges from 35 to more than 1000 W. Metal halide lamps deliver high luminous efficiencies of up to 100 lm/W and good to excellent colour rendition. Lifetime is up to 20 000 h, depending on the type of filling.

A specialty of the lamp types of Fig. 7.17 (right) and Fig. 7.18 (left) is the introduction of a metal halide cycle. This principle is illustrated in Fig. 7.18 (right). When a metal halide lamp first starts, the spectrum is initially that of mercury and starting gas vapor, since the halides remain unevaporated at the cold discharge tube wall. As the wall temperature increases, the metal halides melt and begin to vaporize. Diffusion and convection cause a transport of the vapor species into the hot region of the arc. Here, the halide compounds dissociate into halogen and metal atoms. As shown in Fig. 7.18 (right), different halides dissociate at indicated temperatures. The metal atoms are excited at the hot plasma centre having a temperature of about 5000 K where the main contribution of atomic radiation is emitted. The metal and halogen atoms then move towards colder regions near the discharge wall where they recombine and once again form the halide compound. This cycle repeats itself continu-

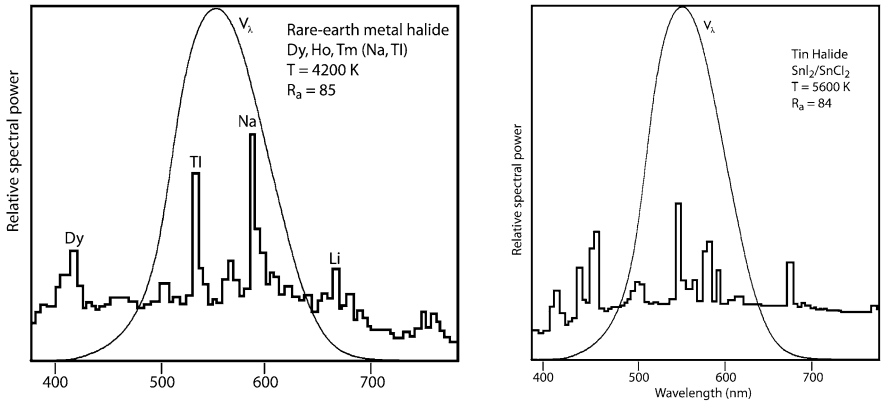

Fig. 7.17. *Left*: spectrum of a NaI/TlI/DyI_3/HoI_3/TmI_3 lamp for sports and flood lighting. *Right*: spectrum of a SnI_2/$SnCl_2$ lamp for studio and theatre lighting

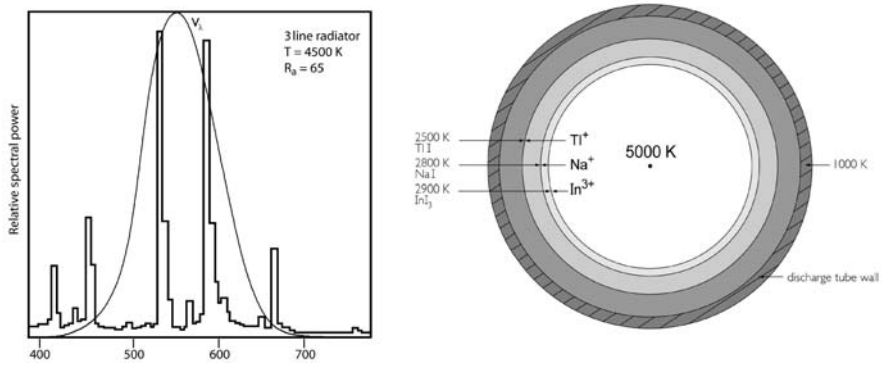

Fig. 7.18. *Left*: spectrum of a three-band colour (NaI, Tl, InI_3) metal halide lamp. The lithium line is due to the presence of impurities in the wall material (quartz). *Right*: schematic diagram of the halide cycle of a three-band colour metal halide lamp (NaI, TlI, InI_3). The values indicate temperatures of wall, arc centre and dissociation of molecules

ously. When adding oxygen and bromine, for example, also a regenerative tungsten cycle can be realized which significantly prevents the lamps from wall blackening.

As already mentioned, a recent improvement of metal halide lamps was achieved by the introduction of polycrystalline alumina (PCA) as a wall material instead of quartz. Such lamps exhibit excellent colour stability and long lamp life. Unfortunately, they are not suitable for optical applications, e.g. in projection systems. The reason is the translucent property of PCA resulting from multiple scattering of photons at grains and pores. Nevertheless, the total transmission for visible light is nearly 95%. Also application of PCA to high power metal halide lamps is limited: cracking of the discharge tube induced by thermal shock and expansion, especially during run-up or when switching off the lamps, is observed. In the lighting industry, the applicability of ceramic wall materials is still an actual field in research and development of modern light sources. Furthermore, upcoming legislation initiated several activities on the replacement of mercury in this type of discharge by non-toxic materials [59]. The first mercury-free metal halide lamp for automotive headlight application was introduced to the market by Philips in 2004.

Other High-Pressure Discharge Lamps

Besides high-pressure mercury and metal halide lamps, the so-called blended-light-lamp is a derivative of the conventional high-pressure mercury lamp. It has a built-in ballast in the form of a tungsten filament connected in series with the discharge. Therefore, radiation from plasma and filament combine (or blend). However, the improved colour property is realized at the expense of reduced system efficiency.

In high-pressure sodium lamps, broadening of the D-lines results in improved colour quality compared to the low-pressure version. Luminous efficiencies of up to 130 lm/W are obtained. Using PCA instead of quartz dramatically improves lamp life and stability of the spectra since it withstands the aggressive Na vapor.

Another class of high-pressure discharge lamps is represented by the sulphur lamp, invented by Turner et al. at FUSION SYSTEMS in 1994. The advantage of this lamp is a long life at high luminous efficiency with electrodeless operation. Sulphur lamps are excited by a microwave generator at a wavelength of 2.45 GHz. The electrical input power is in the order of several kW. The spherical bulb having a diameter of about 30 mm is filled with sulphur powder. At continuous operation, a sun-like white light is emitted by S_2 molecules having a partial pressure of about 600 kPa. High efficiencies of the discharge of about 170 lm/W can be realized since at these pressures UV radiation of the sulphur molecules is reabsorbed by the plasma. Thus, radiation emission mainly occurs in the visible part of the spectrum. A technical drawback of microwave lamps is the quite low energy efficiency of the generator of about 65%. Therefore, the overall efficiency of the system is reduced to about 100 lm/W. Finally, sulphur lamps turned out not to be competitive with conventional metal halide lamps. However, electrodeless discharge lamps are still a hot topic in the lighting industry. One advantage of these systems is their potentially long life due to the lack of plasma interaction with electrodes. Light may be distributed by so-called light engines which are coupled to light guiding pipes. This technique could

Table 7.4. Electrical and light technical data of basic types of visible light sources

Light source	Electrical input power (W)	Luminous flux (lm)	Luminous efficacy (lm/W)	Colour rendering quality
Incandescent	10–1000	80–15 000	8–15	excellent
Halogen	20–2000	300–60 000	15–30	excellent
Low-pressure Hg discharge	7–150	350–15 000	50–100	good
High-pressure Hg discharge	50–1000	2000–60 000	40–60	good
Metal-halide discharge	20–2000	1600–24 000	80–120	good to excellent
Low-pressure Na discharge	20–200	2000–40 000	100–200	poor
High-pressure Na discharge	40–1000	1600–14 000	40–140	moderate to good
Sulphur microwave discharge	up to 5000	up to 450 000	80–90 (system)	good
White dichromatic inorganic LED	1–5	20–150	20–30	good
White trichromatic inorganic LED	1	20–25	20–25	excellent
Organic LED (at 1,000 cd/m^2)	15 mW (per cm^2)	0.25 lm (per cm^2)	15	good

be advantageous for industrial and general lighting applications, e.g. where central light sources are preferred as compared to conventional distributed lighting systems.

7.5.6 General Light Source Survey

Table 7.4 gives a summary over main types of visible light sources together with selected electrical and light technical properties.

7.6 Ultraviolet Light Sources

7.6.1 Introduction

Ultraviolet (UV) light extends from the visible to the X-ray region of the electromagnetic spectrum and is divided in spectral regions UVA, UVB and UVC. This is relevant, e.g. for medical skin treatment and sun tanning studios. The CIE definition is 315 to 400 nm for UVA, 280 to 315 nm for UVB, and 100 to 280 nm for UVC. The region from 200 to 280 nm may be called far ultraviolet (FUV). The term vacuum ultraviolet (VUV) is used for the region 100 to 200 nm. Wavelengths of 105 and 110 nm are the shortest cut-off wavelengths for optical windows (LiF or MgF_2,

respectively) and can be used to distinguish between "extreme ultraviolet" (XUV) with $\lambda < 110$ nm and VUV. Note that the term vacuum ultraviolet may be misleading in the sense that absorption of air sets in at about 200 nm only because of the Schumann–Runge bands (B to X transition) of molecular oxygen and if pure nitrogen or rare gases are used to purge the optical system, electromagnetic radiation may propagate through dense gases without significant absorption down to wavelengths as short as 60 nm, corresponding to the first excitation energy of helium atoms. The expressions deep UV and extreme UV (EUV) are used in photolithography for the VUV and soft X-rays ($\lambda = 13.6$ nm), respectively.

From the various types of UV light sources only portable, sealed-off devices are described here. A broader description of vacuum ultraviolet technology, including e.g. synchrotron sources, can be found in [62] and [63]. Laser induced plasmas are incoherent VUV and XUV sources but will also not be discussed here.

7.6.2 Thermal Tungsten Lamps for Intensity Calibration

Although the intensity of thermal radiation decreases rapidly towards short wavelengths according to Planck's law (see formula (7.1) and Fig. 7.1 in Sect. 7.1.1), there is an important wavelength region around 300 nm in which thermal emitters overlap with other sources such as deuterium lamps, which will be discussed below. This allows intensity calibrations in the UV and VUV regions if an absolutely calibrated thermal emitter is used in combination with a UV light source for which the relative intensities in the emission spectrum is known. The emission of a tungsten strip lamp is shown in Fig. 7.1 together with black body radiation. This lamp is calibrated down to 250 nm, and the emission from deuterium lamps has been calibrated up to 350 nm (see next paragraph). This allows intensity calibration of optical systems from 115 to 2600 nm using these two light sources.

7.6.3 Deuterium Lamps

Deuterium lamps are the most widely used broad-band ultraviolet light sources. Their emission spectrum consists of a combination of several hydrogen molecular bands and continua which are emitted between 120 and 500 nm [63], p. 96. The intensity at wavelengths longer than 350 nm, however, is very low. The Lyman-α line at 121.57 nm is the only pronounced atomic line radiation in the spectrum. The so-called Lyman- and Werner bands which are due to B to X and C to X transitions, respectively, cover the wavelength range from 120 to 130 and 140 to 170 nm, respectively. The structureless continuum at wavelengths longer than 170 nm is due to the radiative decay of the molecular state a ($^3\Sigma_g^+$) to the repulsive b ($^3\Sigma_u^+$) state. A spectrum emitted from a deuterium lamp is shown in Fig. 7.19.

Deuterium lamps are commercially available in various forms as sealed off discharge lamps. Their short wavelength cut-off is determined by the material of the output window. Quartz cut-off is at about 160 nm and MgF_2 at about 110 nm (see Fig. 7.19). The lamps are normally dc arc lamps which are started by use of a hot filament and 300 to 600 V starting voltage. Typical operation conditions are 300 mA

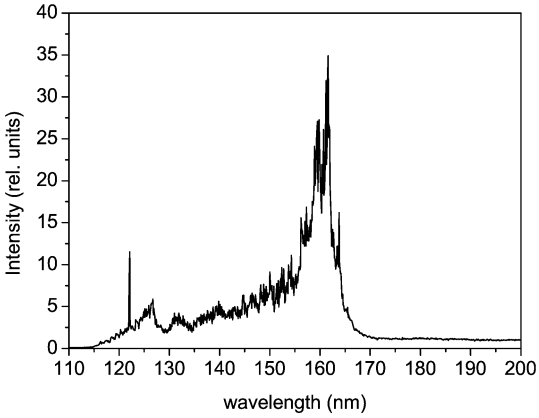

Fig. 7.19. Emission spectrum from a deuterium lamp in the VUV spectral region. The spectrum has not been corrected by the response function of the monochromator detector system. An assignment of the emission bands is given in the text. The line at 121 nm is the Lyman-α line of atomic hydrogen

current and 80 V voltage drop (24 W), and wall plug power is about 100 W. The arc burns between an anode plate and a box-shaped cathode with two openings which define an optical axis. One opening constricts the arc to about 1 mm diameter, and the light is emitted through the second opening of the cathode box. The filament is mounted inside the cathode box, displaced from the optical axis. Besides the standard lamps, water cooled high power devices are available. The shape of the emission spectrum of deuterium lamps has been studied in detail and the spectral radiance of specific deuterium lamps has been tabulated, so that they can be used as transfer standards in the spectral range from 115 to 350 nm [64].

7.6.4 UV Arc Lamps

High-current wall stabilized arc lamps produce an emission spectrum which is a combination of a continuum extending over a wide range in the UV and VUV and line radiation depending on the atoms which are present in the plasma. A light source using a flow of argon at atmospheric pressure has been described in detail in the literature as a transfer standard for spectral radiance [65]. It uses a wall stabilized arc of typically 30 V operating voltage and 50 A current for excitation. The arc is constricted by a 6.3 mm thick water cooled copper plate with a 4 mm diameter hole. The authors provide a table of radiance values between 330 and 114.4 nm and report radiances of, for example, 70 mW/(cm^2 nm sr) at 330 nm and still 6.5 mW/(cm^2 nm sr) at 151 nm for these operating parameters. A more detailed description of the geometry, operating conditions and ways to add different light emitting species to the buffer gas is given in [66]. A wall stabilized arc with a stable radiance on the order of 1 W/(cm^2 nm sr) is described in [67] when xenon was used as the light emitting species.

Arc discharges in sealed off quartz- or ceramic bulbs are usually used for lighting applications. The gas filling is often xenon and mercury with high operating pressures up to 100 bar. They emit a continuous spectrum which resembles a black body spectrum of typically 5000 K radiation temperature with some narrow lines from Hg and Xe on top. The technology of such lamps is described in Sect. 7.5. The UV part of the emission spectrum can be used for simulating the solar spectrum, for example, for testing paints and dyes. Light sources for simulating irradiation by sunlight are commercially available for that purpose.

7.6.5 Mercury Lamps

Although presently the semiconductor industry introduces the ArF laser with a wavelength of 193 nm as light source for photolithography, high-power mercury arc lamps emitting a line dominated spectrum are still of great importance as UV sources in this field, in devices named DUV and i-line stepper. The wavelengths used are 248 and 365 nm, respectively.

Low-power mercury lamps provide the line spectrum shown in Fig. 7.20. The mercury atoms are excited in a low pressure glow discharge with rare gas used as the buffer gas. The concentration of mercury atoms in all mercury lamps is defined by Hg-vapor pressure and therefore by the temperature of the discharge tube. The most widespread application of low-pressure mercury lamps is to provide the ultraviolet light which is converted into visible light in fluorescent lamps. Such light sources are described in detail in Sect. 7.2.2. Some mercury lamps are used as "black lamps" emitting UVA light for fluorescence applications. Fluorescent coatings may be used to shift light emitted in the deep UV to the desired UVA wavelength region, and filters protect the user from the hard UV emitted from mercury.

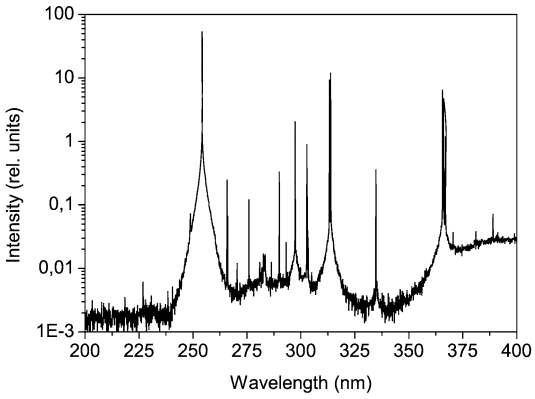

Fig. 7.20. Spectrum of the emission of mercury in the wavelength region 200 to 400 nm. The spectrum was recorded using a small Hg glow discharge lamp for wavelength calibration of monochromator detector systems

Small low-pressure mercury glow discharge lamps with the discharge burning in U-shaped, narrow quartz capillaries are used for wavelength calibration of UV spectrometers (see Fig. 7.20).

7.6.6 Hollow Cathode Lamps

Low-pressure hollow cathode lamps are widely used spectral line sources for atomic absorption spectroscopy in analytical chemistry. They emit a spectrum which is characteristic of the cathode material due to deliberately sputtering the cathode material. Many lines are in the UV part of the electromagnetic spectrum. The lamps consist of a cylindrical cathode and a ring shaped anode inside a glass or quartz tube. A cathode material is introduced to a gas filling of typically 10 mbar neon or argon by sputtering via ions which are accelerated in the cathode fall of the discharge. Line radiation from atoms of about 70 elements, either individually or in combinations, are commercially available via excitation in hollow cathode discharge lamps. The excitation process and technology of hollow cathode lamps is described in more detail in Chap. 4 of [62].

7.6.7 Excimer Light Sources

General Aspects

Excimer light sources are very efficient sources. They cover a wide range of the ultraviolet spectral region and have found their way into practical applications when dielectric barrier discharges were introduced as the excitation method. The excimer light emission process is also of interest for plasma flat panel displays when, for example, dense xenon gas is used as the light emitting species.

Formation and decay of rare gas excimer molecules has been studied for a long time [68, 69]. A schematic energy level diagram for two rare gas atoms versus internuclear distance is plotted in Fig. 7.21. It shows that excited rare gas atoms have an attractive potential and thus can form molecules at elevated gas density via three body collisions.

Rare gas ultraviolet excimer light sources may reach the efficiency of more than 50%. This is due to the favourable energy level scheme and gas kinetics [70]. Briefly, collisional excitation of rare gas atoms leads in a first step to the formation of excited atoms and ions. Ions rapidly form ionic molecules in a dense gas. Molecular ions undergo a so-called dissociative recombination leaving one of the atoms in the ground state and the other in a highly excited state. Highly excited atoms which are either produced by this process or by direct excitation will cascade down to the lowest lying excited states. These states are either metastable or have a long effective lifetime due to radiative trapping of the light in the dense gas. Therefore, essentially all the atoms in the first excited states will form excimer molecules via three body collisions. Excimer molecules decay to the repulsive ground state emitting broad-band continua which cover a wide spectral range from about 60 to 200 nm, as shown in Fig. 7.22. Note that all photons which are emitted from molecular states have a lower energy

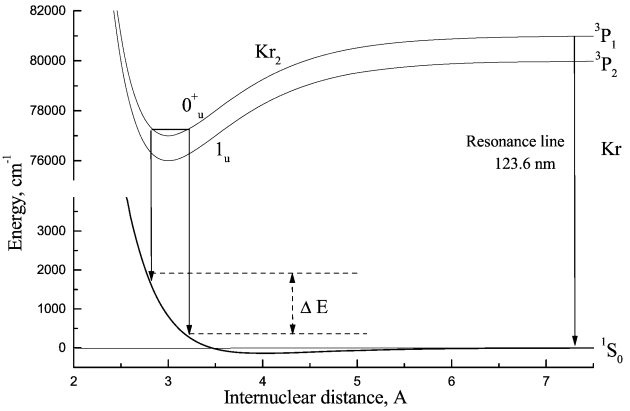

Fig. 7.21. Schematic drawing of a potential energy diagram of the lowest lying levels of two rare gas atoms versus internuclear distance (Kr as an example)

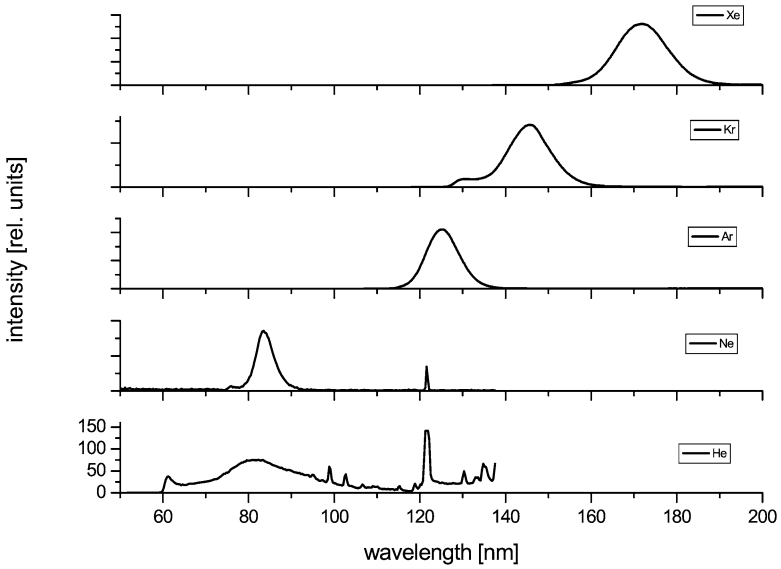

Fig. 7.22. Review of the rare gas emission spectra recorded at a relatively high gas density (gas pressure 1 bar, 1000 hPa)

than photons emitted on the resonance lines of rare gas atoms and are therefore not radiatively trapped in the dense gas.

Emission spectra of rare gas excimer light sources can be strongly modified by using rare gas mixtures and by adding other gases. The reason is that the energeti-

cally high lying levels in rare gas atoms can transfer energy to other species leading to their excitation and ionisation with subsequent emission of light due to transitions in the species which have been added. This effect, however, leads to the problem of pure rare gas excimer lamps that already very low impurity levels can drastically reduce their spectral performance and efficiency. For example, by adding molecular hydrogen on a level of 1%, the neon excimer disappears completely, and the spectrum is dominated by the atomic Lyman-α line at 121.57 nm [71–73]. This example shows that excimer lamps can be easily converted from broad band into narrow band ultraviolet sources and that the emission wavelength can be shifted to longer wavelengths via energy transfer processes. Other examples of ultraviolet sources in which the emission spectrum of rare gases is strongly modified by small admixtures of other gases have been described in the literature: Ar–Xe [74], Kr–Xe [75], Ar–N_2 [76]. The great variety of UV emitting rare gas halogen mixtures used for excimer lasers systems can also be used for incoherent UV and VUV light sources by applying appropriate excitation methods.

Specific Excimer Light Sources

Incoherent excimer light sources have attracted great attention since about 1990. A practical difficulty in designing an excimer lamp is to excite rare gas atoms to energetically high lying levels in a rather cold and dense gas so that the excited species can efficiently form molecules with atoms in the ground state. Pioneering work in the field of excimer lamps was performed by B. Eliasson and U. Kogelschatz using so called dielectric-barrier discharges for exciting dense gases [77]. Earlier work used condensed discharge devices for forming excimer molecules [68]. This approach has been extended very successfully to higher power and the rare gas halide excimers by V. Tarasenko and coworkers [78]. The micro-hollow-cathode discharge was introduced into the field by K.H. Schoenbach et al. [79]. It was also shown that corona discharges can efficiently emit excimer light [80]. Electron beam induced excimer emission can also be produced in compact, portable UV and VUV light sources by using very thin entrance foils for the beam [81].

7.6.8 Excimer Lamps Using Discharge Excitation Glow Discharges

Since glow discharge devices are rugged and easy to use, some powerful incoherent excimer light sources were built using this excitation mechanism. In a particular case a light source was built in the form of two 40 cm long coaxial quartz tubes [82]. The outer tube had an inner diameter of 60 mm, and discharge currents up to 0.5 A were sent through the gap between the outer and inner tube which was either 2.5 or 8 mm wide. The inner tube was used for water cooling of the device. Operating regimes were either high voltages (5 to 7 kV) and low currents (2 to 3 mA) or lower voltages (2 to 3 kV) and higher currents (up to 500 mA). An UV output power up to 130 W was produced with efficiencies on the order of 10%, and was improved to 200 W output and 15% efficiency. Such devices are limited by constriction of the discharge into an arc, a condition under which excimers cannot form.

Dielectric Barrier Discharges

Dielectric barrier discharges (DBD), also called silent discharges, are an excitation method for incoherent excimer light sources [83]. The concept is schematically shown in Fig. 7.23. At least one of two electrodes, which are attached to a gas filled cell, is covered by an insulating material, the dielectric barrier, and an alternating voltage with typically tens of kHz repetition rate and tens of kV amplitude is applied to the electrodes. Capacitive coupling leads to ignition in the gas. Hot streamer discharges develop when the cell is filled with dense gas. But these streamers are stopped already after a few nanoseconds since the dielectric wall charges up due to the current flow in the streamer. In the afterglow phase of the streamer, excimer molecules form from the atoms which were excited and ionized in the streamer phase. Dielectric barrier discharges can be designed to produce only one localized streamer at a time, but normally they make use of a concept where the self-terminating streamer discharges are formed in large quantities randomly in space and time, so that a quasi-homogeneous and quasi-continuous discharge pattern develops. Many parameters such as gas pressure, frequency, and pulse shape of the applied voltage are relevant for dielectric barrier discharge operation. Geometry and size of the devices can be varied over wide ranges and adapted for specific applications. DBD development is an active field of research [84–86].

An advantage of DBDs is that the gas can be kept clean, for example in quartz tubes where it is not in direct contact with the electrodes. Dielectric barrier discharges reach conversion efficiencies of up to 80% light output from power deposited in the discharge volume. The overall efficiency, however, is significantly lower due to the limited coupling efficiency of electrical power into the discharge. This coupling has to be optimized by the electrical design of the device (repetition rate and pulse shape). Small, portable and also large stationary ultraviolet light sources have been built. These devices are the most advanced excimer light sources so far, and are already commercially available from major lighting companies, as UV and VUV sources and also large area, mercury-free visible light sources by using phosphors as wavelength shifters.

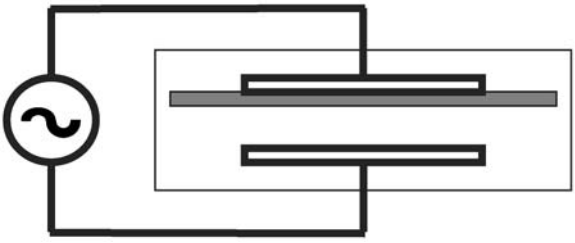

Fig. 7.23. Basic geometry for DBD discharges. Streamer discharges develop between two electrodes. At least one of the electrodes is covered by an insulating material schematically shown as the gray plate next to the top electrode

Micro-Hollow-Cathode Discharges

The use of micro-hollow-cathode discharges (MHC) for excimer light sources has been pioneered by K.H. Schoenbach and his group based on a study of the electrical characteristics of a hollow cathode discharge with small hole diameter (0.7 mm) [87]. The product of gas pressure p and hole diameter D determines the operation regime of the discharge. Successful operation is observed for values which are typically between 0.03 and 13 mbar cm. A light source was demonstrated with argon and xenon at pressures up to one bar and hollow cathodes of 100 µm diameter. Micro-hollow-cathode discharges are appropriate for excimer formation, since the electron energy distribution function reaches up to 100 eV in the cathode fall of this type of discharge, and effective molecule formation is supported by the relatively high gas pressures p which are possible due to the pD scaling of the discharge and small D values. The current–voltage characteristic of the DC- MHC-discharges has a positive slope, so that many MHC discharges can be operated in parallel from the same power supply without electrical interference. The perspective is to build large area, flat UV emitting devices. MHC discharges have also been used with pulsed operation and high instantaneous discharge currents. Due to the high current densities in the narrow, constricted discharge there is a high rate of electrode erosion and spectral lines of the electrode material (e.g. molybdenum) have been observed in the emitted light.

Corona Discharges

A corona discharge can also be used for excimer formation (St. Elmo's fire) [80, 88]. Like a micro-hollow-cathode discharge it is not electrode-less, but the discharge burns more freely between a sharp metal tip and a metal mesh. The operating voltage is of the order of 1 kV and an output power on the second continuum of xenon of 35 mW/cm^2 has been observed with a prototype lamp of 50% efficiency. The needle electrodes used in this setup can also be operated in parallel for designing large area lamps. Needle electrodes have also been used by the same research group with RF-excitation [89]. It could be shown that this reduces electrode erosion significantly, even with very corrosive gases such as ArF and F_2.

7.6.9 Excimer Lamps Using Electron Beam Excitation

Electron beam excitation can provide the non-equilibrium conditions required to populate the rather high lying precursor levels of excimer molecules [90]. All early excimer lasers were pumped by high energy, high current electron beam devices. An advantage of the concept is that there is no feedback between the gas and the excitation process. For example, no ignition conditions depending on gas pressure or gas composition have to be met, and the excitation can have any time structure from short pulses to fully continuous.

A practical issue in all electron beam systems is the separation of the vacuum part where electrons are accelerated from the dense target gas in which the light is produced. Thin metal foils have been used since the early experiments performed

by Lenard in 1894 [91]. Electron beam excitation with very low particle energy has become possible by using extremely thin ceramic membranes as the entrance foils for electron beams [81]. Energy loss of 15 keV electrons in a 300 nm thick SiN_x entrance foil is on the order of 10% [92] and pressures up to several bar can be applied. Time averaged beam current densities of 100 $\mu A/mm^2$ can be sent through the membranes into dense gas targets. The range of the electrons in the heavier rare gases is typically 1 mm. Very compact and brilliant excimer light sources can be built when applying this technique [93, 94]. Efficiencies of excimer light sources of 35% were reached and applications using He and Ne excimer radiation extend to wavelengths below 100 nm [95].

7.7 X-ray-Tubes

7.7.1 History and Generation of X-rays

In October of 1895, Wilhelm Conrad Röntgen (1845–1923), who was professor of physics and the director of the Physical Institute of the University of Wurburg, became interested in the work of Hillorf, Crookes, Hertz, and Lenard. In June 1895 he had obtained a Lenard tube from Muller and had already repeated some of the original experiments that Lenard had created. He reproduced Lenards work generating cathode rays in free air and continued investigating of cathode rays. He modified a Crookes tube fitted with an anode and cathode, separated from each other by a few centimeters in the tube. He used a Rhumkoff induction coil to produce a cathode–anode potential of a few thousand volts knowing that a stream of charged particles would originate in the cathode and would be attracted to the anode.

His first report "On a New Kind of Rays" was published in the Proceedings of the Physical Medical Society of Wuerzburg on December 28, 1895. Not knowing what these emanations were, he uses the term X-ray to describe the rays he was producing. Later, in 1896, he accepted the Rumford gold medal of the Royal Society, and in 1901 he was the first winner of the Nobel Prize in physics.

The characteristics of X-radiation are: invisible, can excite substances to emit light, penetrates matter, cannot be deflected by electric or magnetic fields.

7.7.2 Generation of X-rays

Electron Interaction with Matter. There are 4 basic processes electrons undergo when impinging to matter. Inelastic scattering by photoeffect with ionisation, which lead to emission of characteristic X-radiation and secondary electrons. Auger effect where by internal conversion emitted characteristic X-radiation is absorbed and ionizes an electron from a higher shell. Furthermore, electrons are swinging around the atoms and delivering "Bremsstrahlung" like synchrotron radiation. Elastic scattering generates no X-rays, but changes the direction of the primary electrons.

Fig. 7.24. *Right*: Röntgen. *Left*: the Nobel prize winning photo with the invented X-rays of his wife's hand

Primary electron of high energy suffer inelastic losses by exciting electrons from the shells of the atoms of the sample into higher shells with unoccupied states. Filling the empty level from the next shell above is performed dissipating the energy as electromagnetic radiation. The energy difference determines the frequency and wavelength by

$$\Delta E = h\nu = hc/\lambda. \tag{7.13}$$

Ionizing the K-shell delivers characteristic Kα- and Kβ-radiation.

The generation of "Bremsstrahlung" follow the Duane–Hunts law

$$h\nu_{\max} = hc/\lambda_{\min}. \tag{7.14}$$

Here, $\nu_{\max} = 242 \times 10^{12}$ (Hz). U_{a} (V), with U_{a} the electron acceleration or anode voltage, or $\lambda_{\min} U_{\mathrm{a}} = 12.4 \times 10^{-10}$ (kV m) the lower wavelength limit.

The X-ray lines can be calculated using

$$E_{\mathrm{n}} = -0.5(e^2/4\pi\varepsilon_0)(1/r_H)(Z^2/n^2) = -13.6\ (\mathrm{eV}) \cdot (Z/n)^2. \tag{7.15}$$

A tungsten anode $Z = 74$, k-shell $n = 1$, $eU_{\mathrm{a}} = 745.5$ (keV), delivers by k-shell ionisation and filling of the hole: $h\nu = E_{\mathrm{L}} - E_{\mathrm{K}} = 55.9$ (keV), or $\lambda_{\mathrm{K}\alpha} = 0.022$ nm.

7.7.3 X-ray Filters

Using metal foils of special atomic weight Z, and making use of the fact that X-rays are absorbed in atoms with an effectivity depending on the shell energies. At X-ray energies close to the shell energies, the photoeffect by X-rays changes with a jump, which allows lower energies to pass the filter, but higher energies to be blocked.

X-rays are absorbed by matter of thickness x according to the exponential law of mass absorption

$$I(x) = I_0 \exp(-\mu x). \tag{7.16}$$

For technical applications the mass absorption coefficient μ/ρ and the mass thickness ρx are used, with ρ being the density (kg/cm^3).

According to the mass absorption coefficient μ (cm^{-1}), lead and concrete are used to absorb – shield X-rays in all applications. Here the half-dose thickness $d_{1/2} = \ln 2/\mu = 0.693 x_e$, with $x_e = 1/\mu$ the penetration depth. For example, lead: density $\rho = 11.3$ (g/cm^3), linear attenuation coefficient $\mu = 56.5$ (cm^{-1}), penetration depth $x_e = 0.18$ (mm).

Water has at the same energy the mass attenuation coefficient of $\mu/\rho = 0.2$ (cm^3/g), and the penetration depth $x_e = 5$ (cm). A water layer thickness of $4x_e = 20$ cm absorbs 98.2% of the energy used. The attenuation coefficient is $\approx Z5$.

7.7.4 X-ray Dosimetry

The biological effect of X-rays depends on the number of radiation damages like ionisation events. The dose is proportional to the energy loss divided by the mass. The unit is Gy (Gray).

$$D_e = \Delta E/m \text{ (J/kg)}. \tag{7.17}$$

The ionisation dose $D_i = \Delta Q/m$ (A s/kg).

Formerly the units rad and Roentgen were used:

$$1 \text{ rad} = 10 \text{ mGy} = 10^{-2} \text{ (J/kg) and } 1 \text{ Röntgen} = 2.578 \times 10^{-4} \text{ (A s/kg)}.$$

The mean energy for forming an ion pair is in the range of $w = 27$–34 eV.

The absorption of the energy ΔE produces $\Delta N = \Delta E/w$ ion pairs. With the ionisation constant $k_j = w/e$, one obtains

$$Df = \Delta E/m = w\Delta N/m = w\Delta Q/em = wD_j/m = k_j D_j.$$

In air: D_e (air) = 33.7 V D_j (air).

There is no heating effect in the human body by X-rays. For example, a dose of 10 Gy delivers 10 J to each kg of mass, which converted to heat results in a temperature rise of the body by 2.4 mK, which is negligible. However, 10 Gy is a lethal dose. The natural radiation dose/year is 1 mGy. Tumors are treated in radiation therapy using 30 to 100 Gy, with the radiation applied locally. One X-ray image needs 1–100 mGy.

For radiation – therapy the biological effect depends on the nature of the radiation. Those are classified with factors q describing the relative biological effectivity compared to photons ($q = 1$) and electrons ($q = 1$).

$$\text{The dose-equivalent } D_q = qD_e \text{ (J/kg = Sv); Sv = Sievert.}$$

A dose-equivalent $D_q = 10$ Sv corresponds to a radiation of $q = 10$ radiating to tissue with an energy dose $D_e = 1$ Gy, the biological effect, however, corresponds to an X-ray dose in tissue $D_e = 10$ Gy.

The q-factor for differing radiations are: X-rays, gamma-rays, electrons have $q = 1$; thermal neutrons $q = 3$; fast neutrons (1 MeV) $q = 10$; α-particles (10 MeV); protons (10 MeV) $q = 10$; heavy ions $q = 20$.

7.7.5 X-ray Tubes

Conventional X-ray Tubes

The schematic of an X-ray diffractometre for crystal structure analysis is shown in Fig. 7.25, showing also the schematic of the X-ray tube. The electrons from a thermal electron emitter are accelerated directly to the anode. The beam spot emits then characteristic and Bremsstrahlung. The characteristic radiation of narrow wavelength distribution is used to irradiate the sample. The filter blocks out the Bremsstrahlung to use the characteristic radiation for spectroscopy. A detector, generally a Geiger–Müller detector, is used to count the X-ray photons and amplify the signal by the gas discharge in the counter tube.

The angular position of crystal reflections are governed by the Laue equations and allow to determine the electron density distribution of the elementary cell of the crystal.

X-rays interact with matter by 4 effects. The photo-effect with ionisation; the photo-absorption coefficient is proportional to $Z^4\ E_{-3}$. The Compton effect is inelastic scattering of a photon at a weakly bound outer shell electron of an atom and results in a changed wavelength and changed direction. Pair formation at energy above 1.022 MeV, a photon gets materialized to one electron and one positron. With

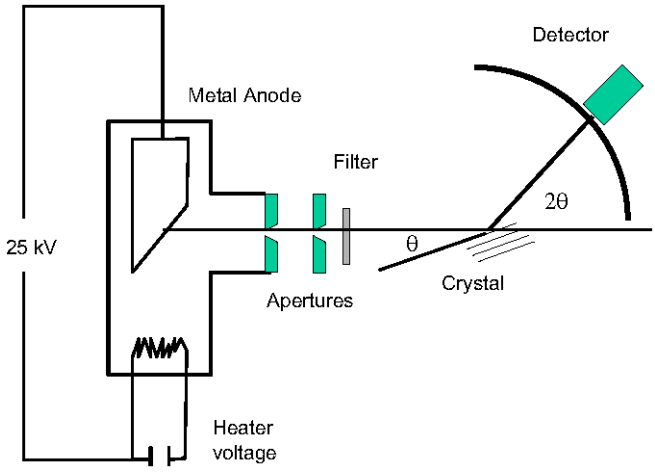

Fig. 7.25. Schematic of an X-ray diffractometer for crystal structure analysis

the Rayleigh scattering it generates radiation perpendicular to the beam which generates dose exposure outside the beam direction.

Figure 7.26 shows a technical tube as supplied by Oxford, showing the electron emitter thermal housing, the anode, and the beryllium window to pass the radiation generated at the fixed or rotating anode to air.

Typical data for a microfocus X-ray tube for analytics are: electron energy 90 kV, beam current 2 mA, total power 80 W, 4 mm anode to object distance, true round spot, grounded target = high power, 80 W, air-cooled. The tube is ideal for X-ray imaging. The tube is designed for those applications where flux density is important. With a true round focal spot and high power loading, it is ideally suited for use with X-ray optics.

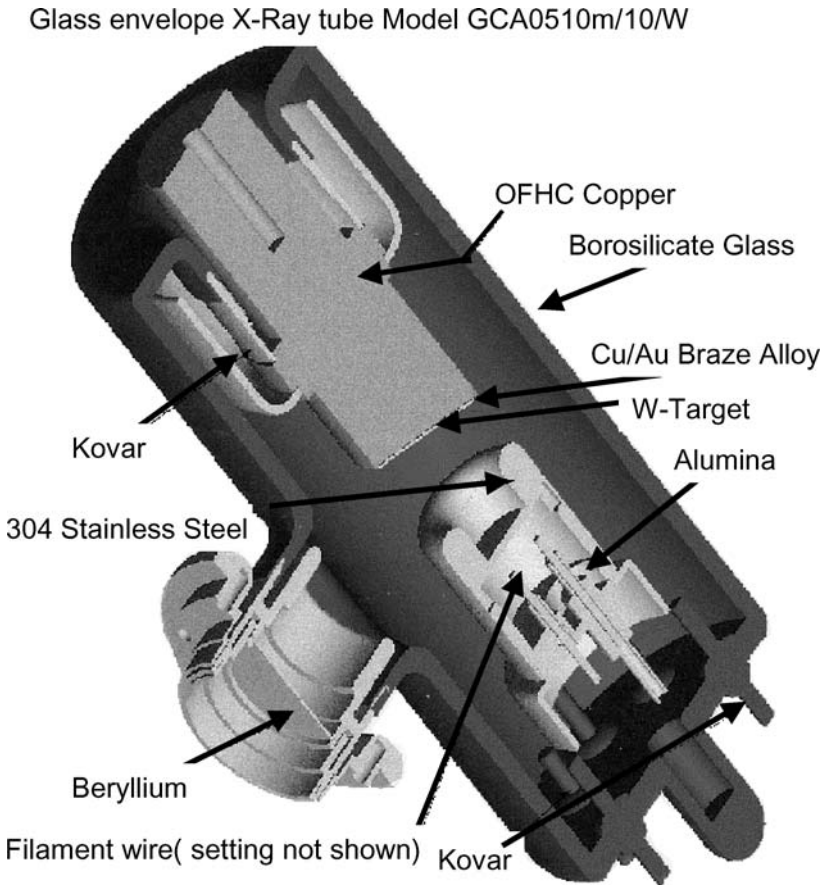

Fig. 7.26. Technical tube as supplied by Oxford, showing the electron emitter thermal housing, the anode, and the beryllium window to pass the radiation generated at the fixed or rotating anode to air

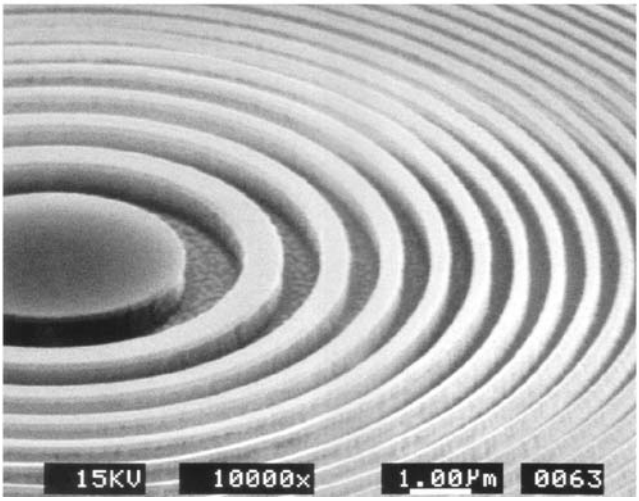

Fig. 7.27. Fresnel zone plate, which is a diffractive grating with variable grating constant, used for focusing

X-ray Optics. Fresnel zone plates, Wolter telescopes, and aspherically polished X-ray mirrors, coated with multiplayer mirrors for high reflection, are the only possibilities to focus X-ray radiation and to generate X-ray images. The semiconductor industry hopes to build chips with the novel Extreme Ultraviolet (EUV) radiation at 13.6 nm. This will help to produce 35 nm CD computer-chip structures in the next 5 years.

Figure 7.27 shows a Fresnel zone plate, which is a diffractive grating with variable grating constant. This has the effect that the first order of the diffracted beam hits in one spot. Therefore, imaging with such X-ray optical elements is possible [96].

7.7.6 Synchrotrons

In physics, the synchrotron radiation, emit electromagnetic radiation by high-speed electrons spiralling along the lines of force of a magnetic field. Depending on the electron's energy and the strength of the magnetic field, the maximum intensity will occur as radio waves, visible light, or X-rays. The emission is a consequence of the constant acceleration experienced by the electrons as they move in nearly circular orbits; according to Maxwell's equations, all accelerated charged particles emit electromagnetic radiation. Although predicted much earlier, the synchrotron radiation was first observed as a glow associated with protons orbiting in high-energy particle accelerators, such as the synchrotron. In astronomy, the synchrotron radiation has been suggested as the mechanism for producing strong celestial radio sources like the Crab Nebula. The synchrotron radiation is employed in a host of applications ranging from solid state physics, lithography for semiconductor industry, LIGA a method to build micromechanical high aspect ratio structures by dell X-ray lithography and

electroforming in the resist mould, and last but not least in medicine. As excellent producers of X-rays, synchrotron sources offer unique probes of the semiconductors that lie at the heart of the electronics industry. Both ultraviolet radiation and X-rays generated by synchrotrons are also employed in the treatment of diseases, especially certain forms of skin cancer. Soft and hard X-rays are used in medical device sterilization, mail sanitation, food pasteurisation and sterilization. Since investment and operation costs for the same quality of irradiation and production capacity are equal for gamma- and X-ray sterilization, the industry has to answer to the challenges, not any longer to rely on cobalt-hard X-ray emitters from nuclear decay in materials, but employ a switchable X-ray source like miniaturized sources in brachiotherapy and other medical internal and external applications, e.g. cancer radiation therapy.

7.7.7 X-ray Detection

X-ray film being specially sensitised for X-rays, is produced in large sheets and is exposed through the object, tooth, body, mechanical structure, etc.

More modern is digital X-ray detection using arrayed X-ray detectors in charged particle devices. These detectors are preferably used in technology, medicine, and astronomy. CXDI-11, an X-ray imaging system, uses the Canon 43 cm $\times$ 43 cm LANMIT amorphous Silicon Sensor System and reaches excellent image quality with more than 7 million detector elements built from amorphous silicon, each of them delivering 4096 grey levels. This allows to compensate for over- and underexposure, and reduces the number of X-ray exposures and repeated exposures.

Immediate image presentation is an especially time saving feature. No costly silver containing plates are required. Images can be transferred and stored, archived, communicated to others electronically, etc.

7.7.8 Applications

Medical: radiography, bone densitometry, X-ray imaging; on-line elemental analysis, particle size analysis; density measurements, process control, inspection, on-line process control; X-ray spectroscopy for materials analysis and composition control, e.g. factories producing concrete are controlled with automated analysis X-ray diffractometers, which determine the concentrations of different materials to be filled into the burning oven.

Electronics/semiconductor: solder joints quality control, MEMS structure control after assembly by bonding. Life sciences: protein and large molecule crystallography, drug discovery and research, “burning” computer chip designs into metal wafers, studying molecule shapes and protein crystals, analyzing chemicals to determine their composition, watching living cells as they react to drugs, fluorescence studies, semiconductor material analysis and structural studies, geological material analysis. Detecting breast cancer tumors is refined by a novel technique that creates three-dimensional X-rays that make tumors much easier to see. Full-field digital tomosynthesis, or TOMO, takes multiple pictures at different angles as the X-ray tube rotates in an arc.

7.7.9 Future Developments: Miniaturized X-ray Tubes

To employ X-ray in medical applications miniaturized tubes are investigated and produced [97, 98]. Micropinches generated in a low inductance vacuum spark (micropinch discharge) are intensive sources of soft X-rays [99]. Brachyo-therapy needs a source of 1 mm diameter and 3 mm in length. Such a source with a thermal emitter and 25 kV delivering 30 μA of current is developed by Xoft [100, 101].

References

[1] G. Kirchhoff, R. Bunsen, Chemische Analyse durch Spectralbeobachtungen, Poggend. Annal. Bd. **110**, S161–169 (1860)
[2] M. Planck, Über das Gesetz der Energieverteilung im Normalspektrum, Drudes Annalen 553 (1901)
[3] J.C. de Vos, A new determination of the emissivity of tungsten ribbon, Physics **XX**, 690–714 (1954)
[4] A.R. Striganov, N.S. Sventitskii, *Tables of Spectral Lines of Neutral and Ionized Atoms* (Plenum, New York, Washington, 1968) (translated from Russian)
[5] Atomic data can also be found on the internet, e.g. at web sites of national bureaus of standard. http://physics.nist.gov/cgi-bin/AtData/main_asd?XXR6000q3000qHgqI
[6] K.P. Huber, G. Herzberg, *Molecular Spectra and Molecular Structure IV Constants of Diatomic Molecules* (Van Nordstrand Reinhold Company, New York, 1979)
[7] W.L. Wiese, *Atomic Transition Probabilities*, vol. I: H through Ne. vol. II: Na through Ca (National Burea of Standards, National Standard Reference Data Series NSRDS-NBS 4, Washington, 1966)
[8] H.S.W. Massey, E.H.S. Burhop, H.B. Gilbody, *Electronic and Ionic Impact Phenomena*, vol. I–V (Clarendon Press, Oxford, 1969–1974)
[9] T.H. Maiman, Stimulated optical radiation in ruby, Nature **187**, 493–494 (1960)
[10] A. Javan, W.R. Bennett Jr., D.R Herriott, Population inversion and continuous optical maser oscillation in a gas discharge containing a He–Ne mixture, Phys. Rev. Lett. **6**, 106 (1961)
[11] C.H. Townes, *How the Laser Happened, Adventures of a Scientist* (Oxford University Press, New York, Oxford, 1999)
[12] D. Eastham, *Atomic Physics of Lasers* (Taylor & Francis, London, Philadelphia, 1989)
[13] B.A. Lengyel, *Lasers*, 2nd edn (Wiley-Interscience, New York, 1971)
[14] R. Beck, W. Englisch, K. Gürs, *Table of Laser Lines in Gases and Vapors* (Springer, Berlin, Heidelberg, New York, 1980)
[15] M.J. Weber, *CRC Handbook of Laser Science and Technology*, vol. II (Gas Lasers) (CRC Press, Boca Raton, 1982)
[16] J.G. Eden (ed.), Selected papers on *Gas Laser Technology*, SPIE Milestone Series, volume MS 159 (SPIE Press, Bellingham, 2000)
[17] R.W. Waynant, M.N. Edinger (ed.), Selected papers on *UV, VUV, and X-Ray Lasers*, SPIE Milestone Series, volume MS 71 (SPIE Press, Bellingham, 1993)
[18] D.L. Matthews, P.L. Hagelstein, M.D. Rosen, M.J. Eckart, N.M. Ceglio, A.U. Hazi, H. Medecki, B.J. MacGowan, J.E. Trebes, B.L. Whitten, E.M. Campbell, C.W. Hatcher, A.M. Hawryluk, R.L. Kauffmann, L.D. Pleasance, G. Rambach, J.H. Scofield, G. Stone, T.A. Weaver, Demonstration of a soft X-ray amplifier, Phys. Rev. Lett. **54**, 110–113 (1985)

[19] J.J. Rocca, V. Shlyaptsev, F.G. Tomasel, O.D. Cortazar, D. Hartshorn, J.L.A. Chilla, Demonstration of a discharge pumped table-top soft-x-ray laser, Phys. Rev. Lett. **73**, 2192–2195 (1994)
[20] A.G. Molchanov, I.A. Poluektov, Y.M. Popov, The possibility of the generation of vacuum ultraviolet radiation by electron excitation of inert-gas crystals, Sov. Phys. Solid State **9**, 2655 (1968)
[21] N.G. Basov, O.V. Bogdankevich, V.A. Danilychev, A.G. Devyatkov, G.N. Kashnikov, N.P. Lantsov, Cathodoluminsecence of solid xenon in the ultraviolet region of the spectrum, JETP Lett. **7**, 317–318 (1968)
[22] P.W. Hoff, J.C. Swingle, Ch.K. Rodes, Demonstration of temporal coherence, spatial coherence, and threshold effects in the molecular xenon laser, Opt. Commun. **8**, 128–131 (1973)
[23] J.B. Gerardo, A.W. Johnson, High-pressure xenon laser at 1730 Å, IEEE J. Quantum Electron. **Q-9**, 748–755 (1973)
[24] C.K. Rhodes (ed.), *Excimer Lasers, Topics in Applied Physics*, vol. 30, 2nd enlarged edn (Springer, Heidelberg, New York, Tokyo, 1984)
[25] C.A. Brau, page 87 in [24]
[26] S.E. Bodner, et al., High gain direct drive target design for laser fusion, Phys. Plasmas **7**, 2298 (2000)
[27] F. Hegeler, M.C. Myers, M. Friedman, J.D. Sehtian, S.B. Swanekamp, D.V. Rose, D.R. Welch, Efficient electron beam deposition for repetitively pulsed krypton fluoride lasers, in *Proceedings of the 14th International Conference on High-Power Particle Beams 2002*, Albuquerque, NM, 23–28 June 2002, p. 357
[28] M. Friedman, S. Swanekamp, S. Obenschain, Y. Chan, L. Ludeking, D. Smithe, Stability of large area electron beam diodes, Appl. Phys. Lett. **77**, 1053 (2000)
[29] F. Hegeler, private communication
[30] G. Marowsky, R. Cordray, F.K. Tittel, W.L. Wilson, C.B. Collins, Appl. Phys. Lett. **33**(1), 60 (1978)
[31] S.J. Smith, E.M. Purcell, Phys. Rev. **92**, 1069 (1953)
[32] T. di Francia, Il Nuovo Cimento **16**, 1085 (1960)
[33] Vermont Electronics homepage. www.vermontphotonics.com
[34] National Research Council, *The Free Electron Laser* (National Academy Press, Washington, 1982); C. Pellegrini, Encyclopedia of Applied Physics **8**, 353 (1994)
[35] M. Goldstein, J.E. Walsh, M.F. Kimmit, J. Urata, C.L. Platt, Appl. Phys. Lett. **71**, 452 (1997)
[36] J.H. Brownell, J. Walsh, G. Doucas, Phys. Rev. E **57**, 1075 (1998)
[37] J. Urata, Spontaneous and stimulated Smith–Purcell radiation experiments in the far infrared, Thesis, Dartmouth College, Hanover, USA, 1997
[38] O. Haeberle, P. Rullhusen, J. Salome, N. Maene, Phys. Rev. E **49**(4), 3340 (1994)
[39] J. Urata, M. Goldstein, M.F. Kimmit, C. Platt, J.E. Walsh, Phys. Rev. Lett. 516 (1998)
[40] J.E. Walsh, J.H. Brownell, J.C. Swartz, J. Urata, M.F. Kimmit, Nucl. Instr. Methods A **429**, 457 (1999)
[41] F. Floreani, H.W. Koops, W. Elsässer, Concept of a miniaturised free-electron laser with field emission source, Nucl. Instrum. Methods Phys. Res. A **483**, 488–492 (2002)
[42] M.J. Moran, X-ray generation by the Smith–Purcell effect, Jpn. J. Appl. Phys. **27**, 408–412 (1988)
[43] M. Schlessinger, *Infrared Technology Fundamentals*, 2 edn. rev. and expanded (Dekker, New York, 1995)
[44] B. Bhanu, I. Pavlidis, *Computer Vision Beyond the Visible Spectrum* (Springer, London, 2005)

[45] K. Stahl, G. Miosga, *Infrarottechnik: Grundlagen, Strah lungssender und Detektoren, Infrarotbildaufnahmen und -wiedergabe, Fernmeßverfahren*, 2 edn (Hüthig, Heidelberg, 1986)
[46] R. Borchert, W. Jubitz, *Infrarotstrahler: zur Erwärmung, Trocknung und Aushärtung, für die Lack-, Textil- und andere Industrien, für die Strahlentherapie*, vol. 5 (Schriftenreihe des Verlages Technik, Berlin, 1951)
[47] E. Martinet, F. Luc, E. Rosencher, P. Bois, E. Costard, S. Delaitre, E. Bockenhoff, in *Intersubband Transitions in Quantum Wells*, ed. by E. Rosencher, B. Vinter, B. Levine (Plenum, New York, 1992), p. 299 (in France)
[48] S.D. Gunapala, S.V. Bandara, *Quantum Well Infrared Photodetector (QWIP) Focal Plane Arrays*. Semiconductors and Semimetals series, vol. 62 (1999)
[49] Shen, et al., Appl. Phys. Lett. **83**, 3118 (2003)
[50] M. Bykhovskaia, et al., Theor. Chem. Acc. **106**, 22 (2001)
[51] P. Han, et al., Opt. Lett. **25**, 242 (2000)
[52] T. Löffler, et al., Opt. Express **9**(12), 616–621 (2001)
[53] Hasegawa, et al., Remote identification of surface texture, Appl. Phys. Lett. **83**, 3996 (2003)
[54] S. Bollaert, et al., Fmax of 490 GHz metamorphic In Al As/In Ga As HEMT's, Electron. Lett. **38**, 389 (2002)
[55] W. Knap, et al., Terahertz emission by plasma waves in 60 nm gate High Electron Mobility Transistor, Appl. Phys. Lett. **48**, 2331 (2004)
[56] R. Köhler, Quantum cascade laser, Nature **417**, 156 (2002)
[57] M. Perrin, et al., JOPA Special Issue on metamaterials
[58] Astafiev, et al., Appl. Phys. Lett. **79**, 1199 (2001)
[59] J.R. Coaton, A.M. Marsden, *Lamps and Lighting* (Arnold and Contributors, 1997)
[60] W. Elenbaas, *Light Sources* (Crane, Russek & Company, Inc., 1972)
[61] M. Born, T. Jüstel, Phys. J. (February), 43 (2003)
[62] J.A. Samson, D.L. Ederer (eds.), in *Vacuum Ultraviolet Spectroscopy*, vol. 1 and vol. 2, Experimental Methods in the Physical Science, vol. 31 (Academic, San Diego, London, Boston, New York, 1998)
[63] J.A.R. Samson, *Techniques of Vacuum Ultraviolet Spectroscopy* (Wiley, New York, London, Sydney, 1967)
[64] Deuterium lamps as transfer standards for spectral radiance in the spectral range 115 nm–350 nm, Physikalisch Technische Bundesanstalt, Inst. Berlin, Abbestr. 2-12, Berlin, Germany, Final report for contract 1405/1/0/002/83/11–BCR–D(30), Sept. 29 (1987); P.J. Key, D.H. Nettleton, Deuterium lamps as transfer standards for spectral radiance measurements, National Physical Laboratory, Teddington, Middlesex TW 11 OLW, UK, Commission of the European Communities BCR information, Applied Metrology Contract No. 615/1/0/002/80/1-BCR-UK(30)
[65] J.M. Bridges, W.R. Ott, Vacuum ultraviolet radiometry. 3: The argon mini-arc as a new secondary standard of spectral radiance, Appl. Opt. **16**, 367–375 (1977)
[66] J.A. Samson, D.L. Ederer (eds.), in *Vacuum Ultraviolet Spectroscopy*, vol. I, chap. 3.4, Experimental Methods in the Physical Science, vol. 31 (Academic, San Diego, London, Boston, New York, 1998)
[67] R.A.B. Zijlmans, J.H. van Helden, D.C. Schram, R. Engeln, The cascaded arc – a novel bright light source for sensitive broadband absorption spectroscopy, P-85, page 355 in Light sources, 2004; G. Zissis, in *Proceedings of the 10th International Symposium on the Science and Technology of Light Sources*, Toulouse, France, 18–22 July 2004, IOP Conference Series Number 182 (Institute of Physics Publishing, Bristol and Philadelphia, 2004)

[68] W. Weizel, Chr. Füchtbauer, Kernschwingungen im Bandenspektrum des Heliums, Z. Phys. **44**, 431–434 (1927)
[69] Y. Tanaka, A.S. Jursa, F.J. LeBlanc, Continuous emission spectra of rare gases in the vacuum ultraviolet region. II. Neon and helium, J. Opt. Soc. Am. **48**, 304–308 (1958)
[70] M.V. McCusker, The rare gas excimers, Chapter 3, in *Excimer Lasers*, 2nd edn., ed. by Ch. Rhodes. Topics in Applied Physics, vol. 30 (Springer, Berlin, Heidelberg, New York, Tokyo, 1984)
[71] J. Wieser, M. Salvermoser, L.H. Shaw, A. Ulrich, D.E. Murnick, H. Dahi, Lyman-alpha emission via resonant energy transfer, J. Phys. B **31**, 4589–4597 (1998)
[72] P. Kurunczi, H. Shah, K. Becker, Hydrogen Lyman-α and Lyman-β emissions from high-pressure microhollow cathode discharges in Ne-H_2 mixtures, J. Phys. B **32**, L651–L658 (1999)
[73] A. El-Dakrouri, J. Yan, M.C. Gupta, M. Laroussi, Y. Badr, VUV emission from a novel DBD-based radiation source, J. Phys. D **35**, L109–L114 (2002)
[74] T. Efthimiopoulos, D. Zouridis, A. Ulrich, Excimer emission spectra of rare gas mixtures using either a supersonic expansion or a heavy-ion-beam excitation, J. Phys. D **30**, 1746–1754 (1997)
[75] A. Morozov, B. Krylov, G. Gerasimov, A. Arnesen, R. Hallin, A study of atomic and molecular energy transfer channels in Kr-Xe gas mixtures excited with radio frequency discharges, J. Phys. B **35**, 1929–1940 (2002)
[76] A. Schmitt, K. Wendt, A. Ulrich, Electron beam pumped UV light source for resonant spectroscopy of atoms, Maier-Leibnitz-Laboratorium für Kern- und Teilchenphysik, LMU and TU Munich, Annual Report 2002, p. 62
[77] B. Eliasson, U. Kogelschatz, UV excimer radiation from dielectric-barrier discharges, Appl. Phys. B **46**, 299–303 (1988)
[78] A.N. Panchenko, E.A. Sosnin, V.F. Tarasenko, Improvement of output parameters of glow discharge UV excilamps, Opt. Commun. **161**, 249–252 (1999)
[79] A. El-Habachi, K.H. Schoenbach, Emission of excimer radiation from direct current, high-pressure hollow cathode discharges, Appl. Phys. Lett. **72**, 22–24 (1998)
[80] M. Salvermoser, D.E. Murnick, High-efficiency, high-power, stable 172 nm xenon excimer light source, Appl. Phys. Lett. **83**, 1932–1934 (2003)
[81] J. Wieser, D.E. Murnick, A. Ulrich, H.A. Huggins, A. Liddle, W.L. Brown, Vacuum ultraviolet rare gas excimer light source, Rev. Sci. Instrum. **68**, 1360–1364 (1997)
[82] M.I. Lomaev, A.N. Panchenko, V.S. Skakun, E.A. Sosnin, V.F. Tarasenko, M.G. Adamson, B.R. Myers, F.T. Wang, Excilamp producing up to 130 W of output power and possibility of its application, Laser Part. Beams **15**, 339–345 (1997)
[83] U. Kogelschatz, J. Salge, High-pressure plasmas: dielectric-barrier and corona discharges – properties and technical applications, in *Low Temperature Plasma Physics*, ed. by R. Hippler, S. Pfau, M. Schmidt, K.H. Schoenbach (Wiley-VCH, Berlin, Weinheim, New York, Chichester, Brisbane, Singapore, Toronto, 2001)
[84] G. Zissis (ed.), Light sources, 2004, in *Proceedings of the 10th International Symposium on the Science and Technology of Light Sources*, Toulouse, France, 18–22 July 2004, IOP Conference Series Number 182 (Institute of Physics Publishing, Bristol, Philadelphia, 2004)
[85] J. Meichsner, D. Loffhagen, H.-E. Wagner (eds.), in *XXVI International Conference on Phenomena in Ionized Gases (ICPIG) 2003*, Greifwald, Germany, July 15–20, 2003 (4 volumes), ISBN 3-00-011689-3
[86] V.F. Tarasenko, G.V. Mayer, G.G. Petrash (eds.), in *Int. Conf. On Atomic and Molecular Pulsed Lasers*, vol. V, Tomsk, Russia, Sept. 15–19, 2003; Proc. SPIE, vol. 5483, SPIE Press, Bellingham, and earlier proceedings of this conference series

[87] K.H. Schoenbach, R. Verhappen, T. Tessnow, F.E. Peterkin, W.W. Byszewski, Appl. Phys. Lett. **68**, 13–15 (1996)
[88] M. Salvermoser, D.E. Murnick, Efficient, stable, corona discharge 172 nm xenon excimer light source, J. Appl. Phys. **94**, 3722 (2003)
[89] M. Salvermoser, D.E. Murnick, Stable high brightness radio frequency driven microdischarge lamps at 193 (ArF^*) and 157 nm (F_2^*), J. Phys. D **37**, 180–184 (2004)
[90] C.A. Brau, Rare gas halogen excimers, Chapter 4 (4.3), in *Excimer Lasers*, 2nd edn., ed. by Ch.K. Rhodes. Topics in Applied Physics, vol. 30 (Springer, Berlin, Heidelberg, New York, Tokyo, 1984)
[91] P. Lenard, Ueber Kathodenstrahlen in Gasen von atmosphärischem Druck und im äussersten Vacuum, Annal. Phys. Neue Folge Band **51**, 225–267 (1994)
[92] R. Gauvin, P. Hovongton, D. Drouin, P. Horny, H. Demers, CASINO program (public domain) Université de Sherbrooke, Québec, Canada. http://www.gel.usherb.ca/casino/
[93] M. Salvermoser, D.E. Murnick, J. Wieser, A. Ulrich, Energy flow and excimer yields in continuous wave rare gas-halogen systems, J. Appl. Phys. **88**, 453–459 (2000)
[94] F. Mühlberger, J. Wieser, A. Ulrich, R. Zimmermann, Single photon ionization (SPI) via incoherent VUV-excimer light: robust and compact time-of-flight mass spectrometer for on-line, real-time process gas analysis, Anal. Chem. **74**, 3790–3801 (2002)
[95] A. Fedenev, A. Morozov, R. Krücken, S. Schoop, J. Wieser, A. Ulrich, Applications of a broadband electron-beam pumped XUV radiation source, J. Phys. D **37**, 1586–1591 (2004)
[96] G. Schmahl, D. Rudolf (eds.), *X-ray Optics and Spectroscopy* (Plenum, New York, 1987)
[97] H.H. Busta, J.M. Chen, Z. Shen, K. Jansen, S. Rizkowski, J. Matey, A. Lanzillotto, Characterization of electron emitters for miniature X-ray sources, J. Vac. Sci. Technol. B **21**(1), 344 (2003)
[98] H.H. Busta, in *Vacuum Microelectronics,* Chap. 7, ed. by W. Zhu (Wiley, New York, 2001), p. 315
[99] O.G. Semyonov', A.E. Gurey, A.P. Kanavin, A.A. Tikhomirov, Applications of micropinch x-ray source, J. Vac. Sci. Technol. B: Microelectron. Nanometer Struct. **19**(4), 1235–1240 (2001)
[100] Xoft microTube, Inc., homepage
[101] R. Nath, L.L. Anderson, G. Luxton, et al., Dosimetry of interstitial brachytherapy sources: Recommendations of the AAPM Radiation Therapy Committee Task Group 43, Med. Phys. **22**, 209–234 (1995)